JOURNAL OF PETROLOGY | VOLUME 39 | NUMBER 3 | PAGES 495–517 | 1998

Petrogenesis of Carbonatite Magmas from Mantle to Crust, Constrained by the System $CaO–(MgO + FeO^*)–(Na_2O + K_2O)–(SiO_2 + Al_2O_3 + TiO_2)–CO_2$

WOH-JER LEE* AND PETER J. WYLLIE

DIVISION OF GEOLOGICAL AND PLANETARY SCIENCES, CALIFORNIA INSTITUTE OF TECHNOLOGY, PASADENA, CA 91125, USA

RECEIVED APRIL 15, 1997; REVISED TYPESCRIPT ACCEPTED OCTOBER 21, 1997

Experimental results from the systems $CaO–MgO–SiO_2–CO_2$, $Na_2O–CaO–Al_2O_3–SiO_2–CO_2$, and a primitive magnesian nephelinite mixed with carbonates have been combined for construction of phase diagrams for the pseudoquaternary system $CaO–(MgO + FeO^*)–(Na_2O + K_2O)–(SiO_2 + Al_2O_3 + TiO_2)$ with CO_2 at 1·0 and 2·5 GPa pressure. These diagrams provide a petrogenetic framework for magmatic processes from mantle to deep crust, with particular reference to the melting products of carbonate peridotite and the paths of crystallization of carbonated silicate magmas toward carbonatite magmas, with or without the intervention of silicate–carbonate liquid immiscibility. Three key features control these processes: (1) the liquidus surface bounding the silicate–carbonate liquid miscibility gap, (2) the silicate–carbonate liquidus boundary surface which separates the liquidus volume for primary silicates from that for primary carbonates, and (3) the curve of intersection of these two surfaces (1 and 2) which defines the coprecipitation of silicates and calcite with coexisting immiscible silicate- and carbonate-rich liquids. The geometrical arrangement of the two surfaces varies as a function of both pressure and bulk composition (e.g. with Si/Al, Na/K, Mg/Fe). Surface (2) is the locus of initial liquids from partial melting of carbonate–silicate assemblages, and the limit for residual liquid compositions derived from silicate–CO_2 liquids. The carbonate liquidus volume is a forbidden region for carbonate-rich magmas derived from silicate magmas at the pressures investigated. The immiscible liquids dissolve no more than 80 wt % $CaCO_3$, and the miscibility gap (MG) becomes smaller with increasing Mg/Ca. Extrapolation of experimental data indicates that the MG disappears with more than ~50 wt % (MgO + FeO) at 1·0 GPa for the compositions investigated. The distance between the miscibility gap, surface (1), and the silicate–carbonate liquidus surface, surface (2), increases significantly with increasing (MgO + FeO*). This observation, coupled with knowledge of the phase boundaries in the system, allows comparisons with projected rock compositions, and this permits the following conclusions. Calciocarbonatites and natrocarbonatites are excluded as candidates for primary magmas from the mantle, which must have compositions dominated by calcic dolomite. The formation of (equilibrium) carbonate-rich liquids immiscible with silicate magmas in the mantle is unlikely, which denies the formation of $CaCO_3$ ocelli in mantle xenoliths as immiscible liquids. Immiscible carbonate-rich magmas separated from many silicate magmas may tend to be concentrated near calciocarbonatite compositions, with maximum $CaCO_3$ 75–80 wt %, low (MgO + FeO*), and $(Na,K)_2CO_3$ near 15 wt %. Silicate parents with higher Na/Ca and peralkalinity may yield immiscible magmas approaching natrocarbonatite compositions. Exsolution of immiscible carbonate-rich magma occurs without the coprecipitation of calcite except along the limiting field boundary (3). Only after the carbonate-rich magma is physically separated from the parent magma, and cooled with the precipitation of silicates, does it reach the silicate–carbonate field boundary and precipitate cumulate carbonatites, with inevitable enrichment of residual liquids in alkalis. Calciocarbonatite magmas cannot be derived from natrocarbonatite magmas. Dolomitic carbonatite magmas cannot be formed by liquid immiscibility, but only by fractionation of calciocarbonatites (according to $CaCO_3–MgCO_3$), or as primary magmas.*

KEY WORDS: *$CaCO_3$ ocelli; carbonatite; liquid immiscibility; nephelinite*

*Corresponding author. Telephone: +1 (818)-395-6239. Fax: +1 (818)-568-0935. e-mail: wjl@gps.caltech.edu

INTRODUCTION

Although carbonate-rich melts are rare among igneous magmas, their occurrences and consequences may be dramatic. There is evidence in xenoliths for the presence of carbonates in the mantle (e.g. Pyle & Haggerty, 1994; Kogarko *et al.*, 1995; Ionov *et al.*, 1996), and growing evidence for the role of carbonate-rich melts in mantle metasomatism (e.g. Haggerty, 1989; Barker, 1996*a*; Ionov *et al.*, 1996). Petrological and geochemical evidence has been presented for the eruption of primary carbonatite magmas directly from the mantle (e.g. Bailey, 1993), for the extrusion of calciocarbonatite magmas (e.g. Keller, 1981, 1989), and for an origin by liquid immiscibility of the only observed carbonatite lava flows, the natrocarbonatites of Oldoinyo Lengai (e.g. Church & Jones, 1995; Dawson *et al.*, 1996). The association of carbonatites with nephelinite volcanism is well established (e.g. Le Bas, 1977; Bell & Keller, 1995), but there is also evidence that residual carbonate-rich melts may be produced through crystallization of ultrabasic magmas such as kimberlites (e.g. Dawson & Hawthorne, 1973; Donaldson & Reid, 1982; Exley & Jones, 1983; Jones & Wyllie, 1985). Experimental evidence has been adduced for the formation of carbonate-rich melts from subducted oceanic crust (e.g. McInnes & Wyllie, 1992; Nichols *et al.*, 1994), and in the overlying mantle wedge (Sweeney *et al.*, 1992), but we are not aware of any petrological or geochemical evidence to support these proposals.

Debates about the interpretation of field, petrological, and geochemical evidence for the origin of carbonatites have been summarized elsewhere (e.g. Bell, 1989; Bailey, 1993; Lee & Wyllie, 1994, 1996; Bell & Keller, 1995; Barker, 1996*b*). Major questions remain controversial for most stages of the evolution paths of carbonatitic magmas, including the generation of carbonate-rich liquids or carbonated silicate liquids within the mantle, their modification as they are transported into the crust, and their differentiation within the crust before their emplacement in subvolcanic structures. Particular questions are concerned with the following: (1) Are carbonatite magmas formed in the mantle or in the crust? (2) Is the composition of primary (from the mantle) or parental carbonatite magma dolomitic, calcic, or sodic? (3) Are carbonatite magmas derived from silicate magmas by fractional crystallization or by liquid immiscibility? (4) What is the petrogenetic relationship between magmas which form sövites or rauhaugites?

Changes in rock names and definitions, and the use of rock names to describe magmas, may lead to confusion unless the differences among the terms are defined and maintained. Sövites and rauhaugites are igneous rocks with mineralogy dominated by calcite or dolomite, respectively, now commonly described as calciocarbonatites or magnesiocarbonatites: CaO-rich–calcitic, or rich in (CaO + MgO)–dolomitic [see Woolley & Kempe (1989) for classifications]. Calciocarbonatite (sövitic) and magnesiocarbonatite (rauhaugitic) magmas are those which produce the corresponding rocks. Another potential source of confusion is the use of liquid compositions in phase diagrams to simulate paths of crystallization followed by the liquids in magmas; a magma consists of (liquid + minerals). As discussed below, many intrusive carbonatites involve crystal settling, and the magmas which precipitated the rocks may have compositions differing significantly from the rocks themselves.

Phase equilibrium experiments with model systems and natural rocks provide constraints on petrogenetic processes, illustrating which processes are possible, and which appear to be impossible. The paths of crystallization in model systems, and the resultant parageneses and liquid compositions so derived, do not correspond precisely in terms of temperature and phase compositions to minerals and liquids in complex whole-rock systems. But rock systems are complex, and it is not always easy to decipher the phase relationships throughout the temperature interval of interest, especially in systems where liquids do not quench to homogeneous glasses. Phase relationships for a specific rock composition represent one path through a multicomponent system, and considering the diversity of igneous rock compositions, there are many different paths to be determined. A multicomponent model phase diagram, although not representing precisely individual rock compositions, provides the broad framework of phase fields through which individual magma paths must pass, and complements and facilitates interpretation of the whole-rock experimental studies. Experiments have confirmed that carbonatite magmas may be generated through one of the following mechanisms: (1) by partial melting of carbonated peridotites (e.g. Wyllie & Huang, 1975, 1976*a*; Eggler, 1978; Wallace & Green, 1988), (2) by crystal fractionation of some silicate–CO_2 magmas (e.g. Franz & Wyllie, 1967; Watkinson & Wyllie, 1971; Otto & Wyllie, 1993; Lee & Wyllie, 1994), and (3) by liquid immiscibility of other silicate–CO_2 liquids (e.g. Koster van Groos & Wyllie, 1973; Freestone & Hamilton, 1980; Kjarsgaard & Hamilton, 1988, 1989*a*; Kjarsgaard & Peterson, 1991; Kjarsgaard *et al.*, 1995).

Furthermore, the phase diagrams illustrate that these three processes are not mutually exclusive, and carbonatite genesis may involve some combination of them.

Most applications of previous liquid immiscibility studies in model systems have taken an experimentally determined isobaric isothermal section through the miscibility gap and compared this with the compositions of magmas or rocks. Kjarsgaard & Peterson (1991) and Kjarsgaard *et al.* (1995) in addition reported isobaric polythermal crystallization sequences from immiscible

liquids, based on experiments using natural rock compositions. Lee & Wyllie (1992*a*, 1992*b*, 1996, 1997*a*, 1997*b*) have emphasized that these approaches are rarely sufficient to understand igneous processes; it is necessary to define the silicate and carbonate liquidus fields on either side of the miscibility gap, and the field boundaries traversing them. This paper is one of our series of papers developing the phase relationships related to silicate–carbonate liquid immiscibility in progressively more complex systems in the pressure range from 2·5 GPa (mantle conditions) to 1·0 GPa (deep crustal conditions). Liquidus volumes, surfaces, and field boundaries are projected into a pseudoquaternary system CaO–(MgO + FeO*)–(Na_2O + K_2O)–(SiO_2 + Al_2O_3 + TiO_2) with CO_2 (FeO*: total iron expressed as oxide), which includes most of the major and minor elements important in the petrogenesis of alkaline igneous rocks and carbonatites. The tetrahedron provides a generalized phase diagram emphasizing the relationships between the miscibility gap and the silicate–carbonate field boundary. The positions of magmas and rocks projected into this experimental framework provide definitive insights into possible and impossible processes associated with the relationship of carbonatite magmas to silicate rocks and magmas, from the upper mantle to the crust.

THE MISCIBILITY GAP AND THE SILICATE–CARBONATE LIQUIDUS FIELD BOUNDARY

The pseudoquaternary phase relationships are constructed from the experimental results in simpler systems, starting with the triangular Hamilton projection for Na_2O–CaO–(Al_2O_3 + SiO_2) which is shown in Fig. 1 (Lee & Wyllie, 1994, 1996). The key petrogenetic features are the liquid miscibility gap, and the silicate–carbonate liquidus field boundary. The nature of changes produced in the relative positions of key phase boundaries as a function of pressure, and of changes in composition (Al/Si or Ne/Ab), is illustrated in Fig. 2. The effect of MgO on the silicate–carbonate liquidus field boundary without liquid immiscibility is shown in the model mantle system CaO–MgO–SiO_2–CO_2 (Fig. 3; Wyllie & Huang, 1976*a*). Results from our experiments with MgO-bearing natural nephelinite and dolomite (Baker & Wyllie, 1990; Lee & Wyllie, 1997*a*) are incorporated into the pseudoquaternary tetrahedron CaO–(MgO + FeO*)–(Na_2O + K_2O)–(SiO_2 + Al_2O_3 + TiO_2) with CO_2 in Figs 4–6.

System Na_2O–CaO–Al_2O_3–SiO_2–CO_2

From the phase fields intersected by the joins $NaAlSi_3O_8$–$CaCO_3$ (Ab–CC) and $NaAlSiO_4$–$CaCO_3$ (Ne–CC) at 1·0–2·5 GPa, Lee & Wyllie (1996, 1997*b*) determined the phase relationships in two slices through the tetrahedron Na_2O–CaO–Al_2O_3–SiO_2 (+ CO_2), and presented them in the pseudoternary Hamilton projection, Na_2O–CaO–(Al_2O_3 + SiO_2). Figure 1 shows the result at 1·0 GPa obtained from the albite join. Measured compositions of coexisting liquids at 2·5 GPa confirm that the immiscibility phase relationships are nearly ternary. This is also true for the miscibility gap intersected by the nepheline join. The crystallization of silicate minerals with compositions off the triangular slices causes the liquids to diverge from the triangles, and the phase relations then cease to be ternary.

Figure 1 shows the key features of the phase relationships which control the paths of crystallization of carbonated magmas, or of progressive fusion of carbonated rocks. Arrows in the direction of decreasing temperature give an indication of the thermal structure of the liquidus surface. The miscibility gap (two-liquid field, straight-lined area) is covered by a high-temperature liquidus dome, rising from the liquidus surfaces for primary silicates (light shading) and primary carbonates (stipple). The intersection between the miscibility gap liquidus dome and the liquidus surfaces is given by the liquidus field boundary m–f–k–g–n, showing the compositions of the silicate-rich liquids (Ls, along m–f–k) which coexist with a carbonate-rich liquid (Lc, n–g–k), a vapor, and a mineral phase. Point k is the critical point where Ls = Lc, marking a temperature maximum on the field boundary. The silicate and carbonate liquidus fields meet along the field boundary for the coprecipitation of silicates and carbonates, and this is divided into two sections, e–f and g–o, because it intersects the miscibility gap. The miscibility gap is occupied by two-liquid tie-lines subparallel to f–g, which is the special tie-line for immiscible liquids coexisting with vapor and two minerals, silicate and calcite.

The silicate and carbonate liquidus surfaces are divided into primary fields, few of which have been delineated. One incomplete field boundary for coexisting albite and wollastonite was located. There is an extensive liquidus field for primary calcite extending from the CaO apex. The carbonate liquidus surface extends in a narrow band g–o–Na_2O, with primary sodium carbonate at the Na_2O corner, and Ca–Na-carbonate compound(s) in between (e.g. nyerereite; Cooper *et al.*, 1975).

Effect of Al/Si, Mg/Ca and pressure on liquidus field boundaries

Figure 2a corresponds to Fig. 1, where the silicate–carbonate liquidus field boundary (e–f, g–o) intersects the miscibility gap (m–f–k–g–n). Lee & Wyllie (1997*b*) determined the effect of Al/Si on the major phase fields,

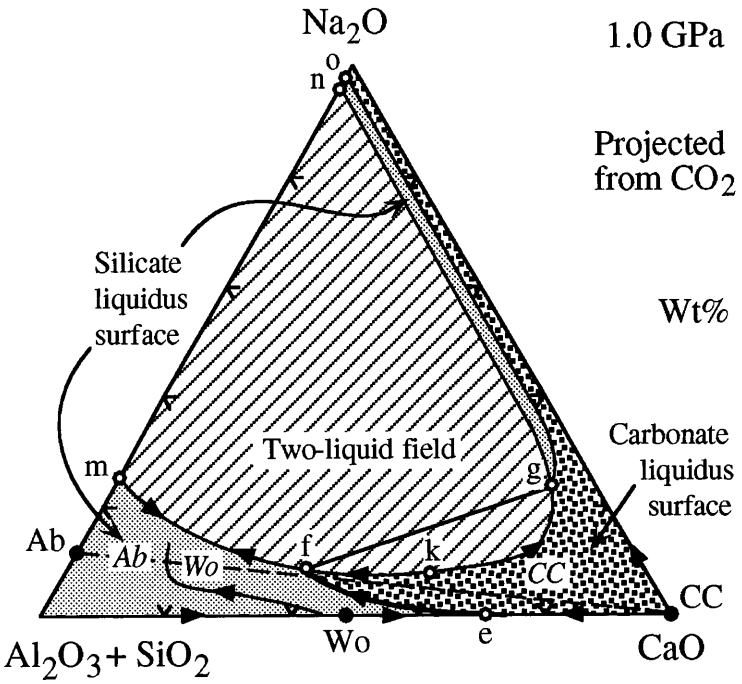

Fig. 1. Pseudoternary phase relationships for the system Na_2O–CaO–Al_2O_3–SiO_2–CO_2 at 1·0 GPa in the Hamilton projection (based on albite–calcite), showing the silicate–carbonate two-liquid field, silicate liquidus field, and carbonate liquidus field, which are separated by the miscibility gap field boundary m–f–k–g–n, and the two sections of the silicate–carbonate liquidus field boundary e–f and g–n (Lee & Wyllie, 1996). Arrows indicate the cooling directions. ●, compositions for $NaAlSi_3O_8$ (Ab), $CaSiO_3$ (Wo), and $CaCO_3$ (CC). Italic characters *Ab*, *Wo* and *CC* indicate the liquidus minerals albite, wollastonite and calcite. (Note there is another field boundary within the silicate liquidus surface between Ab and Wo.)

comparing the results intersected by two composition joins at 1·0 GPa: Ab–CC (Al/Si = 1/3), and $Ne_{90}Ab_{10}$–CC. The latter join is situated near the plane Ne–CC–NC (Al/Si = 1) in the tetrahedron Na_2O–CaO–Al_2O_3–SiO_2 (+CO_2). Figure 2c represents schematically their experimental results for the Ne–CC join at 1·0 GPa. Whereas the size of the miscibility gap does not change significantly with increasing Al/Si, the calcite liquidus field becomes substantially smaller, with the result that there are changes in the relative positions of the two key liquidus field boundaries of Fig. 1. The silicate–carbonate liquidus field boundary e–f moves toward the carbonate side, and the points f and g approach each other (Fig. 2a). The tie-line f–g becomes shorter as the points f and g approach the critical point k. At one particular condition, as sketched in Fig. 2b, the points f and g must become coincident with k, with the two sections of the liquidus field boundary, e–f and g–o, merging and sharing a common tangent at k with the miscibility gap field boundary. With further change, the two field boundaries become separated (Fig. 2c), and the silicate liquidus surface then surrounds the miscibility gap. The silicate–carbonate boundary e–f–g–o, and the miscibility gap field boundary, m–f–k–g–n, intersect in Fig. 1 for the join Ab–CC (e.g. Fig. 2a), but they become completely separated for the join Ne–CC (e.g. Fig. 2c).

Within the tetrahedron Na_2O–CaO–Al_2O_3–SiO_2 at constant pressure, the field boundaries of the Hamilton projection in Figs 1 and 2 extend into surfaces. These two surfaces meet in a curve, which is generated by the points f and g as they migrate across the surface enclosing the miscibility gap with increasing Al/Si, with the crest of the intersection curve being k(fg) in Fig. 2b. Similar changes are associated with changes in pressure and other compositional parameters (e.g. Mg/Ca).

Lee & Wyllie (1996) demonstrated a significant pressure effect on the size of the three phase fields shown in Fig. 1, and on the geometrical arrangement of the field boundaries. With decreasing pressure, the miscibility gap becomes smaller, suggesting that perhaps at pressures lower than 1·0 GPa the geometry of the system could change from that of Fig. 2a through the special condition of Fig. 2b to the condition of Fig. 2c.

Baker & Wyllie (1990) and Lee & Wyllie (1997*a*) determined the miscibility gap in a magnesian system, using a primitive (magnesian) nephelinite (NEPH) mixed with (Ca,Mg,Na)-carbonate between 2·5 and 1·0 GPa. These compositions have Al/Si ~1/3, ~2·7 wt % TiO_2,

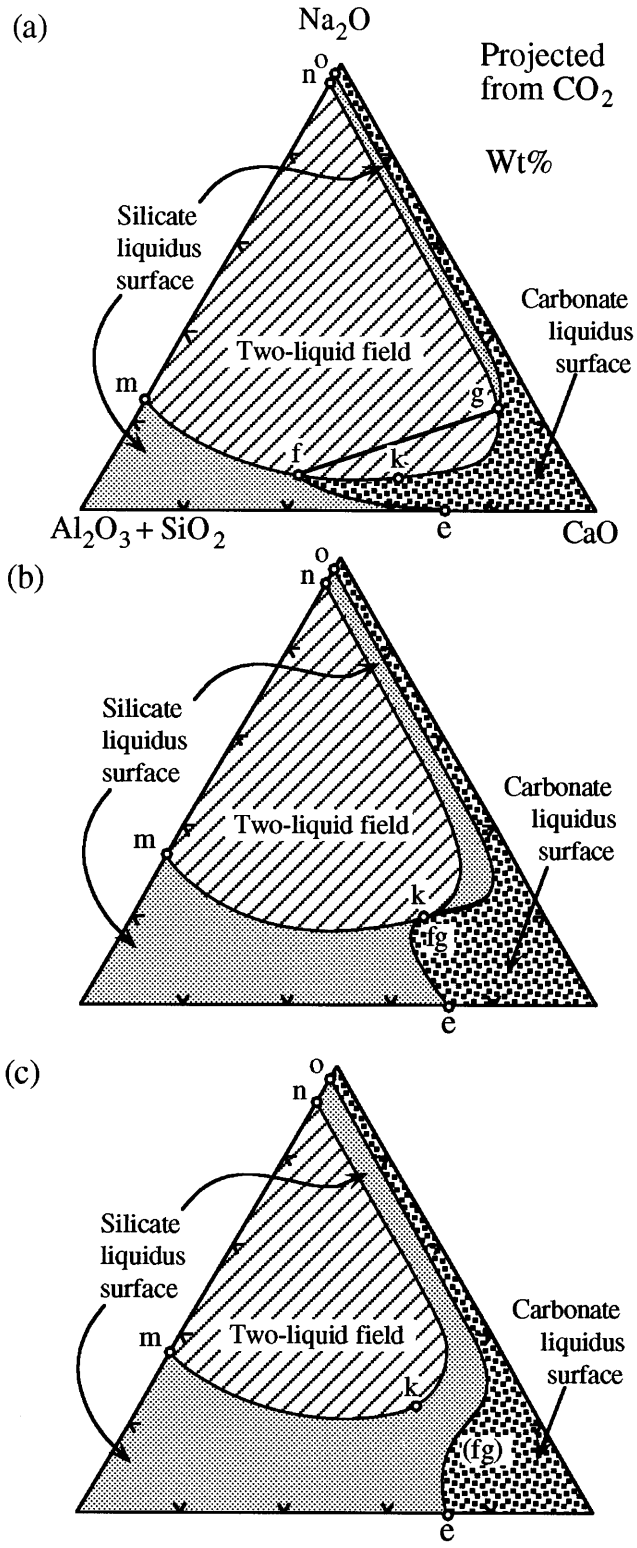

Fig. 2. Variation of the geometrical arrangement of phase field boundaries as a function of composition (e.g. Al/Si) or pressure. (a) The silicate–carbonate liquidus field boundary (e–f, g–n) intersects the miscibility gap field boundary (m–f–k–g–n), as in Fig. 1. (b) The liquidus field boundary is tangential to the miscibility gap field boundary. (c) The two field boundaries are separated from each other. The change in the arrangement from (a) to (c) results from the increase in Al/Si of the system, or the decrease in pressure. Notice that (a) is real (see Fig. 1), but (b) and (c) are versions distorted so that the changing relationships among phase elements can be seen.

and ~1·0 wt % K_2O, but they differ from those in Fig. 1 mainly in Mg and Fe contents. The differences in the major phase fields and boundaries between the two systems may therefore be due largely to the Mg and Fe in the NEPH system. Lee & Wyllie (1997*a*) compared the NEPH results with those for the Mg-free system of Figs 1 and 2a (Lee & Wyllie, 1996). The size of the miscibility gap decreases with increasing Mg/Ca at constant pressure. They also determined that the silicate–carbonate liquidus field boundary in magnesian system studied does not intersect the miscibility gap, indicating that the geometry (between 1 and 2·5 GPa) corresponds to that in Fig. 2c. Therefore, considering the tetrahedron formed from Fig. 2a by adding (MgO + FeO*) as an apex, the changing intersection of the two surfaces with increasing Mg/Ca at constant pressure follows the same sequence as for increasing Al/Si, or for decreasing pressure, i.e. from Fig. 2a, through Fig. 2b to Fig. 2c.

Petrological applications

Lee & Wyllie (1996) used Fig. 1 to illustrate the evolution of silicate–CO_2 parental liquids. Liquids on the surface m–f–e–(Al_2O_3 + SiO_2) may follow crystallization paths (1) directly to the miscibility gap (curve m–f) with the exsolution of carbonate-rich liquids (g–n), (2) to the liquidus field boundary (curve e–f) for the coprecipitation of silicate and calcite, or (3) to a terminal silicate–CO_2 eutectic for precipitation of silicates with evolution of a vapor phase. The immiscible carbonate-rich liquids (Lc) along g–n do not precipitate carbonates; they must first separate from their consolute silicate liquids (Ls) and cool down the liquidus surface g–n–o, precipitating silicates, until they reach the silicate–carbonate liquidus field boundary g–o. Figure 1 also shows that at 1·0 GPa, MgO-free immiscible carbonate-rich liquids can dissolve no more than ~80 wt % $CaCO_3$. The existence of ~99 wt % $CaCO_3$ immiscible liquids thought to be responsible for the formation of calciocarbonatites (Kjarsgaard & Hamilton, 1988, 1989*a*; Brooker & Hamilton, 1990) is thus ruled out (confirmed by Kjarsgaard, fig. 5 of Macdonald *et al.*, 1993). The limit is even more restricted for derivatives of silicate–CO_2 liquids. Initial silicate-precipitating liquids can exsolve carbonate-rich liquids with compositions only along g–n; the maximum dissolved $CaCO_3$ in derivative liquids in Fig. 1 is therefore ~70 wt % $CaCO_3$.

PSEUDOQUATERNARY DIAGRAM CaO–(MgO + FeO*) – (Na_2O + K_2O)–(SiO_2 + Al_2O_3 + TiO_2)

The decrease of Mg/Ca in carbonate-rich melts from the dolomite-dominated liquid produced from carbonate peridotite in the mantle compared with the dominant calciocarbonatites in the crust is significant. Similarly, Mg/Ca decreases as primary magnesian silicate-rich melts in the mantle fractionate during their uprise and emplacement into the crust. This compositional variation can be illustrated in a tetrahedron (Figs 4 and 5) formed by adding an (MgO + FeO*) apex to an expanded Hamilton projection CaO–(Na_2O + K_2O)–(SiO_2 + Al_2O_3 + TiO_2) (compare Figs 1 and 2). The phase relationships which we construct below at 1·0 GPa must be considered as generalized pseudoquaternary interpretations, because the effects of Al/Si, Fe/Mg, Na/K and Mg/Ca on the field boundaries are not fully determined, and cannot be represented in the tetrahedron.

The results in Fig. 1 determined from the Ab–CC join through system Na_2O–CaO–Al_2O_3–SiO_2–CO_2 provide phase relationships for one face of the tetrahedron. The effects of Mg/Ca on the silicate–carbonate field boundary can be shown in the bounding triangle CaO–MgO–SiO_2, in the presence of CO_2. Phase relationships on the other two triangles are estimated. Lee & Wyllie (1997*a*) determined the effect of Mg/Ca on the size of the miscibility gap inside the tetrahedron. Combination of these data defines the topology of the two liquidus surfaces for (1) the immiscible liquids, and (2) the silicate–carbonate boundary.

The experiments involving silicate–carbonate joins include regions where a separate vapor phase is formed (CO_2), and regions where the liquid is undersaturated with CO_2. The distribution of these regions, i.e. the boundary between vapor present and vapor absent in the phase elements, varies as a function of bulk composition and pressure (vapor-absent region increasing as pressure increases). An indication of the geometry of these variations has been given in many papers (e.g. Huang & Wyllie, 1974; Maaloe & Wyllie, 1975; Huang *et al.*, 1980). We make no attempt to map out this boundary in the tetrahedron, because we do not know its location in all places, the geometry is far too complicated, and it would add little to our conclusions. The positions of the phase elements between 1·0 and 2·5 GPa will shift somewhat from those with vapor present as the CO_2 content is decreased in vapor-absent experiments, but we believe that the topology (in this pressure range) will not be significantly affected. The note by Brooker & Holloway (1997) indicates a large effect for CO_2 variation.

The system CaO–MgO–SiO_2–CO_2

The main features of the phase relationships in CaO–MgO–SiO_2–CO_2 are fairly well known (e.g. Wyllie & Huang, 1975, 1976*a*; Eggler, 1976, 1978; Canil & Scarfe, 1990; Dalton & Wood, 1993; Dalton & Presnall, 1995,

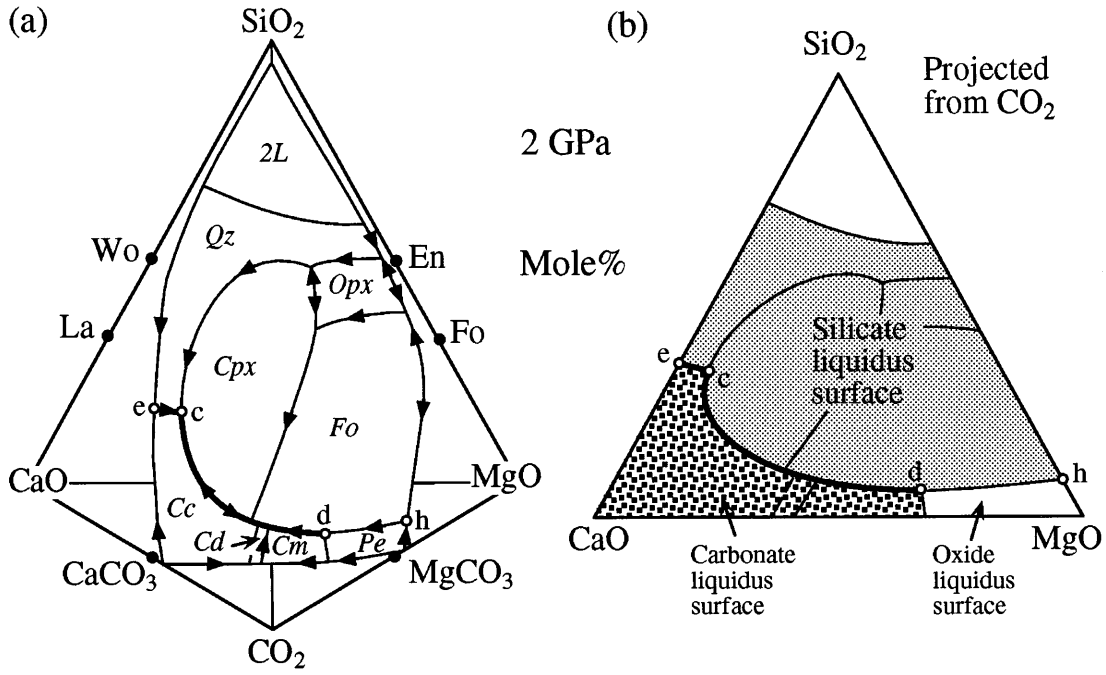

Fig. 3. (a) Schematic quaternary phase diagram (by mol %) at 2 GPa (after Wyllie & Huang, 1976*a*), showing the CO_2-saturated liquidus surface in the system CaO–MgO–SiO_2–CO_2, with the liquidus fields for silicates (Qz, Cpx, Fo, and Opx), carbonates (solid solutions: Cc, Cd, and Cm), and oxide (Pe). Arrows indicate the cooling directions; ●, ideal compositions of selected phases. The silicate–carbonate field boundary is shown by the heavy curve e–c–d, and the silicate–oxide boundary by d–h. 2L near the SiO_2 corner marks the oxide–oxide two-liquid field. Qz, quartz; Cpx, clinopyroxene; Fo, forsterite; Opx, orthopyroxene; En, enstatite; Wo, wollastonite; La, larnite; Cc, calcite; Cd, dolomite; Cm, magnesite; Pe, periclase. (b) Liquidus fields and boundaries in (a) projected onto the CO_2-free triangle CaO–MgO–SiO_2.

1996). Wyllie & Huang (1976*a*) mapped out the CO_2-saturated liquidus surface at various pressures. Their schematic diagram for 2 GPa is reproduced in Fig. 3a, with a simplified projection from CO_2 to the triangle CaO–MgO–SiO_2 in Fig. 3b, which distinguishes only silicate, carbonate and oxide liquidus surfaces. A noteworthy feature is the large silicate liquidus surface including the primary minerals clinopyroxene, forsterite, quartz and orthopyroxene (Cpx, Fo, Qz, Opx). The liquidus fields for primary carbonates, solid solutions of calcite, dolomite and magnesite (Cc, Cd, Cm), are in contact with the silicate liquidus surface along the heavy line e–c–d. This silicate–carbonate field boundary terminates at d, because at this pressure, carbonate is replaced by periclase (Pe, oxide) on the higher-temperature, more magnesian liquidus. The area marked 2L shows the high-temperature oxide–oxide liquid miscibility gap, not the silicate–carbonate immiscibility relevant to this study.

The extent and arrangement of phase fields in Fig. 3 varies with pressure. The point d approaches h with increased pressure, and periclase is completely replaced by magnesite at some pressure <2·7 GPa (Irving & Wyllie, 1975; Wyllie & Huang, 1976*a*, fig. 11). With increasing pressure, the Opx field extends between Cpx and Fo to reach the silicate–carbonate field boundary, whereas the Cpx field shrinks (Wyllie & Huang, 1976*a*). The Opx field reaches the dolomite liquidus, bringing calcic dolomite (70 wt % $CaCO_3$ + 30 wt % $MgCO_3$; Wyllie *et al.*, 1983, fig. 5) into equilibrium with the melting peridotite assemblage Fo + Opx + Cpx + L + V at ~2·8 GPa in the model system, and 2·0–2·2 GPa in natural dolomite–peridotite (Wallace & Green, 1988; Wyllie & Rutter, 1986, in Wyllie, 1987). At lower pressures, a liquidus field for wollastonite occurs between Qz and Cc (Huang *et al.*, 1980). The carbonate liquidus surface may become somewhat smaller with decreasing pressure, but we assume that the topology is preserved, with the silicate–carbonate liquidus field boundary curving away from the CaO ($CaCO_3$) corner to reach a field boundary such as e–c.

The bounding pseudoternary phase relations

The tetrahedron CaO–(MgO + FeO*)–(Na_2O + K_2O)–(SiO_2 + Al_2O_3 + TiO_2) has been folded open in Fig. 4 to show the critical field boundaries for the four bounding triangles at 1·0 GPa. The base of the tetrahedron shows the field boundaries from Fig. 1. The field

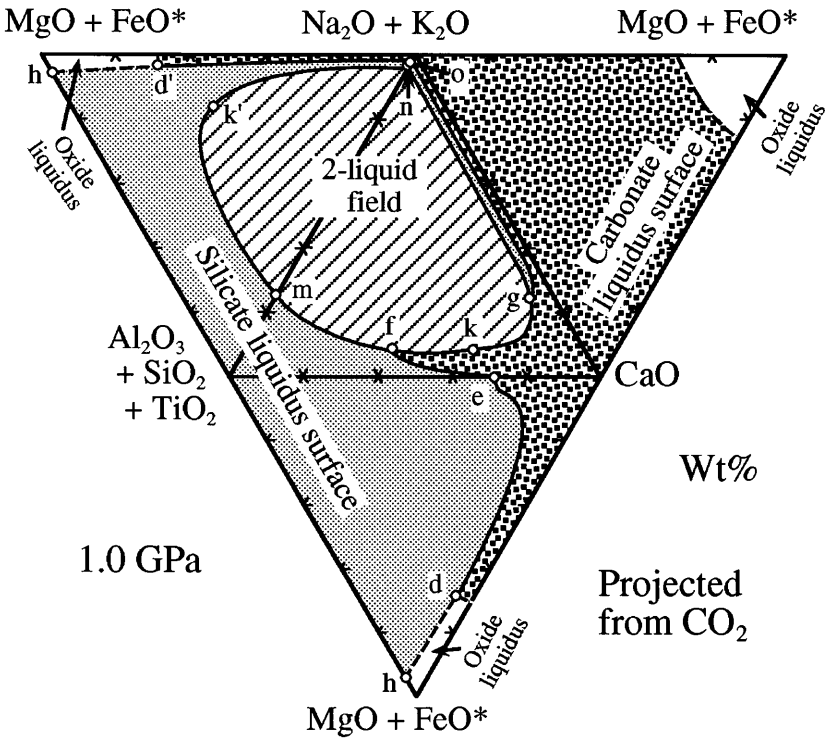

Fig. 4. Field boundaries intersected by the end-member triangles of the tetrahedron CaO–(MgO + FeO*)–(Na_2O + K_2O)–(SiO_2 + Al_2O_3 + TiO_2), projected from CO_2, at 1·0 GPa. Three major fields are defined for the silicate–carbonate liquid miscibility gap (two-liquid field), silicate liquidus surface, and carbonate liquidus surface. The phase relationships for the central triangle are from Fig. 1. The boundary h–d–e in the lower triangle is estimated based on higher-pressure results of Wyllie & Huang (1976*a*), as in Fig. 3. In the upper-left triangle, curve m–k′–n is constrained by points m and n, and by data within the tetrahedron (Lee & Wyllie, 1997*a*; see Fig. 5); curve h–d′–o is limited by points h and o. A small oxide field near the (MgO + FeO*) apex is also sketched. (See text and previous figures for points d, e, f, g, h, k, m, n, and o.) k′ is the critical point for the CaO-free miscibility gap m–k′–n. Point d′ between the carbonate and oxide fields in the CaO-free triangle corresponds to d.

boundary h–d–e for the system CaO–MgO–SiO_2–CO_2 is similar to that for 2 GPa in Fig. 3, with minor adjustment for the lower pressure, and recalculation to weight per cent.

The triangle CaO–(MgO + FeO*)–(Na_2O + K_2O) with CO_2 is the carbonate end-member of the system. Known carbonate melting relationships include Na_2CO_3–K_2CO_3–$CaCO_3$ at 0·1 GPa by Cooper *et al.* (1975), and $CaCO_3$–$MgCO_3$–CO_2 up to 3·6 GPa (Irving & Wyllie, 1973, 1975; Huang & Wyllie, 1976; Byrnes & Wyllie, 1981). The liquidus surface at high pressures is dominated by primary carbonates, with a small area for oxides near MgO, as shown, sketched to correspond to the carbonate–oxide boundary from d.

There are no experimental data for the end-member system (MgO + FeO*)–(Na_2O + K_2O)–(SiO_2 + Al_2O_3 + TiO_2), but the topology must correspond to that in Fig. 4. Limiting points are m, n, and o from Fig. 1, and h is based on Fig. 3. The silicate–carbonate liquidus field boundary extending from point o toward h surely remains subparallel to the axis (MgO + FeO*)–(Na_2O + K_2O). Point d′, where the oxide liquidus field replaces carbonate, is located to correspond to the position of d. The closure of the miscibility gap at critical point k′ is estimated by extrapolation of the results of Lee & Wyllie (1997*a*) from within the tetrahedron, which will be summarized in connection with Fig. 5.

Figure 4 shows the distributions of the bounding areas for the silicate, carbonate, and miscibility gap liquidus fields, and the field boundaries between them. The corresponding phase elements are connected within the tetrahedron by volumes and surfaces, respectively. It should be noted that the oxide liquidus field is replaced by the expanding magnesite liquidus before the pressure reaches 2·7 GPa.

The pseudoquaternary phase relations

Lee & Wyllie (1997*a*) determined the effect of MgO on the miscibility gap within the tetrahedron at 1·0 GPa (Figs 4 and 5). The curve A–A in Fig. 5, the 1200°C isotherm for a composition join involving the magnesian nephelinite (NEPH), encloses an area considerably smaller than does the curve B–B, the corresponding isotherm

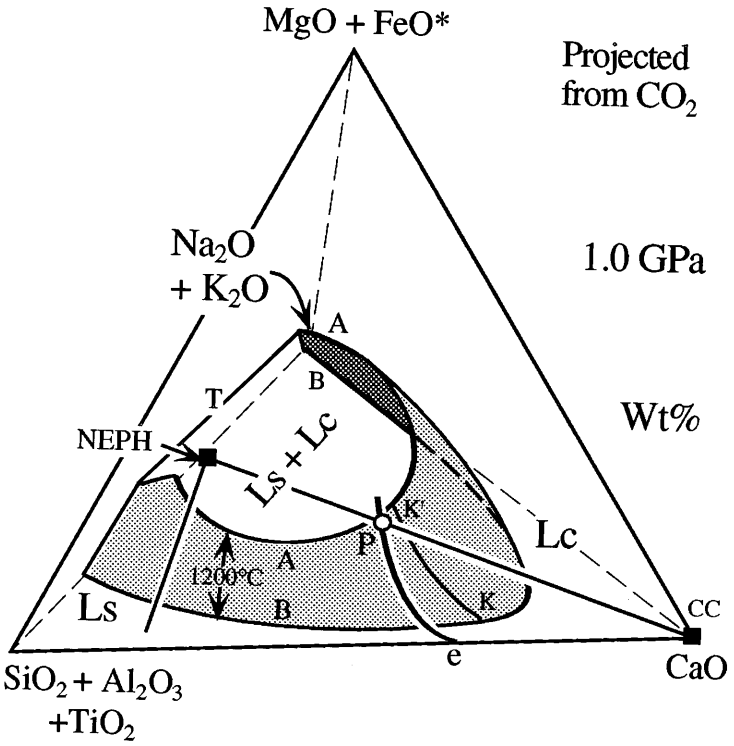

Fig. 5. Experimental data illustrated in the tetrahedron of Fig. 4, showing two-liquid isotherms A–A (magnesian) and B–B (Mg-free) at 1200°C and 1·0 GPa (based on Lee & Wyllie, 1997*a*). The shaded area between A–A and B–B illustrates the isothermal surface enclosing the miscibility gap, with line K–K′ showing the critical curve where Ls = Lc. T is a two-liquid tie-line in the Ca-free triangle. Point P is the intersection of the olivine and calcite liquidi along the join NEPH–CC at 1 GPa (Lee & Wyllie, 1997*a*). Curve e–P is a polythermal silicate–carbonate liquidus field boundary (compare e–f, Fig. 1), lying on the surface defining compositions of liquids which coprecipitate silicate and carbonate minerals. NEPH is the nephelinite 68KEE-1 from Hawaii (Clague & Frey, 1982), and its spatial position is illustrated by the thin line projected through (MgO + FeO*) to the basal triangle. Ls, silicate-rich liquid. Lc, carbonate-rich liquid.

in the MgO-free system (close to the field boundary m–f–k–g–n in Fig. 4). The shaded area connecting B–B and A–A is the 1200°C isothermal liquidus surface enclosing the miscibility gap. Geometrically, it is not far removed from the miscibility gap liquidus surface with field boundaries and primary minerals, which is the extension of the field boundary m–f–k–g–n (Fig. 4) into three dimensions. This surface is reproduced in Fig. 6a, and extrapolated to closure on the bounding triangle (MgO + FeO*)–(Na_2O + K_2O)–(SiO_2 + Al_2O_3 + TiO_2). Its estimated shape is shown by the contours of constant (MgO + FeO*) wt % (see Fig. 6c for numerical values). The critical curve for Ls = Lc connects k (Figs 1 and 4) through the critical point on A–A (Fig. 5, see Lee & Wyllie, 1997*a*), to the extrapolated point k′ near ~50 wt % (MgO + FeO*); this is the value plotted in Fig. 4.

Point P (Fig. 5) is a liquidus piercing point for coexisting calcite and olivine determined on the composition join NEPH–CC by Lee & Wyllie (1997*a*). The curve connecting P to e (defined on the base of the tetrahedron, Figs 1 and 4) is therefore a line on the silicate–carbonate liquidus boundary. This curve constrains the position of the silicate–carbonate liquidus surface which connects the bounding curves e–d, e–f, and o–g (Fig. 4) within the tetrahedron, as illustrated in Fig. 6b. No attempt has been made to draw the position of e–P in Fig. 6b, but visualization of its position indicates that the surface rising from e–f on the triangular base is convex upwards, remaining fairly close to the front triangle CaO–(MgO + FeO*)–(SiO_2 + Al_2O_3 + TiO_2) before sweeping around to approach the side triangle CaO–(MgO + FeO*)–(Na_2O + K_2O). Its position in space is shown by the contours for constant (MgO + FeO*) wt % (see Fig. 6c for numerical values). The area h–d–d′ shows the silicate–oxide liquidus surface, and the oxide is replaced by carbonate below d–d′. Following the surface downward, it is subparallel to the carbonate end-member triangle, until at ~30 wt % (MgO + FeO*) near the CaO corner, where the size of the primary carbonate volume starts to increase. The surface then bends sharply to connect with the surface rising from e–f.

The relationship between the two surfaces at 1·0 GPa is shown in the completed Fig. 6c. The surfaces overlap

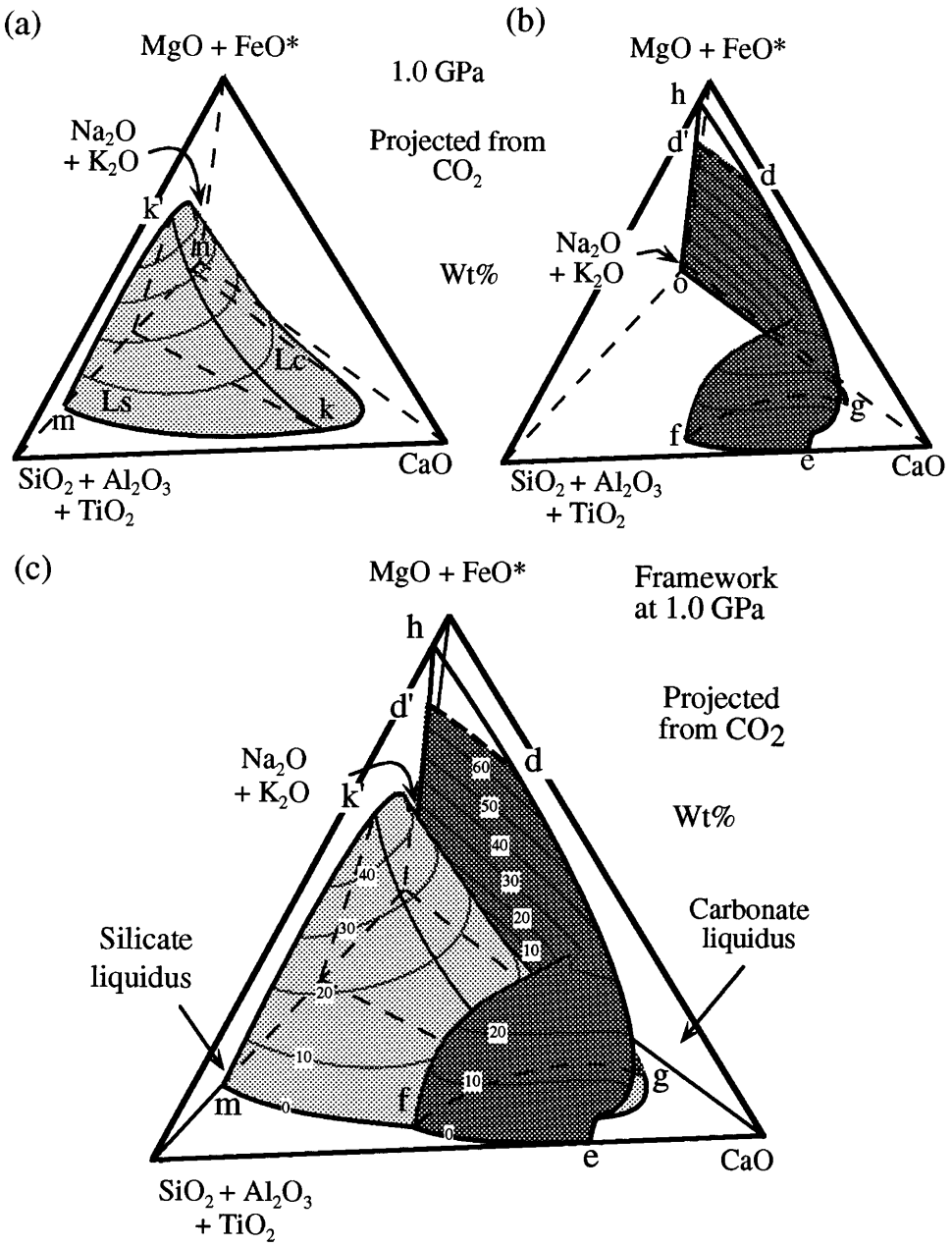

Fig. 6. Partly schematic phase relationships constructed in the tetrahedron at 1·0 GPa (based on the data in Figs 4 and 5), showing the three major liquidus volumes for the miscibility gap, silicate liquidus field, and carbonate liquidus field, and the liquidus surfaces between them. Contours and values for wt % (MgO + FeO*) of the surfaces are also shown. (a) and (b) illustrate separately the miscibility gap surface, and the silicate–carbonate field boundary surface, respectively. (c) shows the completed pseudoquaternary phase diagram which combines the results in (a) and (b). [See Fig. 4 for the key construction points (e.g. m, n, o).]

on the base of the tetrahedron along f–g in Figs 1 and 2a, and intersect along the dashed line f–g within the tetrahedron (Fig. 6b and c). They divide the space within the tetrahedron into three major volumes, the liquid miscibility gap (i.e. immiscibility volume), the silicate liquidus, and the carbonate liquidus. The geometrical changes with increasing (MgO + FeO*) can be envisioned considering Fig. 2a–c as sections through the tetrahedron for specific contours in Fig. 6c. Figure 2a represents a low value of (MgO + FeO*) intersecting the dashed curve f–g; Fig. 2b is the special case for the contour giving the maximum (MgO + FeO*) along

dashed line f–g; and Fig. 2c corresponds to higher (MgO + FeO*) where the two surfaces have separated.

Within the silicate liquidus volume, the primary minerals change with increasing (MgO + FeO*) from felsic minerals, including albite, anorthite, wollastonite, and nepheline (Fig. 1; Lee & Wyllie, 1996, 1997*b*), to pyroxene in the intermediate range, and olivine in the most magnesian domain (Figs 3 and 4; Wyllie & Huang, 1976*a*; Lee & Wyllie, 1997*a*). The carbonate liquidus volume is subdivided into the fields for calcite, dolomite, and magnesite, as in Fig. 3, and calcite, nyerereite and Na_2CO_3 in Fig. 1, but the details inside the volume remain undetermined. The carbonate volume is replaced near the (MgO + FeO*) apex with the small oxide (periclase) volume (adjacent to h–d–d′).

The space within the miscibility gap is filled with tie-lines connecting immiscible liquids. Immiscible liquids do not have the same (MgO + FeO*) concentrations, i.e. they do not connect points on the same contour lines. Examples of magnesian two-liquid compositions (on a CO_2-free basis) at 1·0–2·5 GPa have been given by Lee & Wyllie (1997*a*, table 3).

The distribution of phase elements in the tetrahedron Fig. 6 is based on experimental compositions which we believe represent normal conditions in the upper mantle and deep crust. In contrast, Kjarsgaard & Hamilton (1989*b*) reported at 0·6 GPa the coexistence of a melilititic liquid and a magnesian carbonate-rich liquid (with 9·3 wt % SiO_2, 10·9% MgO, 4·2% FeO*, 29·2% CaO, 3·6% Na_2O, 2·3% K_2O, ~35% CO_2, and other minor components), with the two-liquid tie-line in different orientation from those presented above. Kjarsgaard (1997) described experimental conjugate liquids at 0·2–2·5 GPa involving melilititic and magnesian sövitic (12% MgO, 30% CaO) compositions, but noted that 'high CO_2 contents were utilized, and it is unclear from existing partial melting studies of carbonated peridotite if magmas of this composition are possible'. P. Ulmer (personal communication, 1997) also has experimental results on MARID compositions indicating an enlarged immiscibility volume for compositions containing MgO and high K_2O.

The effect of pressure

We emphasize that the sizes and relative arrangements of the phase elements in Fig. 6 change as a function of pressure and composition (e.g. Fig. 2), but they do not disappear. Figure 7 shows how the geometry of the two surfaces changes with increased pressure to 2·5 GPa. For the Mg-free system on the base of the tetrahedron, the size of the miscibility gap (curve B–B, Fig. 5) increases, and the position of the silicate–carbonate field boundary (e–f) extends much closer to the CaO-free point m (Lee & Wyllie, 1996). This is associated with significant enlargement of the calcite liquidus field, and movement of the tie-line f–g away from calcite. In addition, the magnesian miscibility gap (curve A–A, Fig. 5) decreases in size (Lee & Wyllie, 1997*a*). The size of the unshaded area h–d–d′, the silicate–oxide liquidus surface, also decreases at higher pressures, with periclase being replaced by magnesite at some pressure less than ~2·7 GPa.

We expect more rapid geometrical changes at low pressures, and it appears that the immiscibility volume in Fig. 6 would have steep walls, i.e. its cross-section would not decrease as rapidly with increasing Mg/Ca. [See the 0·6-GPa magnesian two-liquid compositions of Kjarsgaard & Hamilton (1989*b*).]

PETROLOGICAL APPLICATIONS

Figures 7–9 compare rock compositions relevant to carbonatite magmatism with the generalized pseudo-quaternary phase relationships expressed in the tetrahedron of Fig. 6. The examples cover pressure and temperature conditions ranging from the mantle to crust. The phase relationships are sketched at two pressures: 2·5 GPa, representing deep lithospheric mantle (Fig. 7), and 1·0 GPa, representing deep continental crust (Figs 8 and 9). Visualization of the positions of rock compositions plotted within the tetrahedron is facilitated by means of the thin lines projected from (MgO + FeO*) through the data points to the basal triangle. The location of each composition with respect to the phase surfaces is readily distinguished in each diagram by these projection lines, and by the label for weight per cent of (MgO + FeO*) adjacent to each point, compared with the (MgO + FeO*) contours on each surface.

Silicate magmas are represented by the small volume for alkali basalts (e.g. Frey *et al.*, 1978) and the primitive magnesian nephelinite (NEPH), which are situated well within the silicate liquidus field, away from both the immiscible liquids and the silicate–carbonate co-precipitation liquidus boundary (Fig. 7). Melilitites (e.g. Brey, 1978) projected into Fig. 7 overlap the right side of the alkali basalt volume, extending downward for more evolved compositions to ~20 wt % (MgO + FeO*) (Le Bas, 1977). Kimberlites (e.g. Mitchell, 1989) project above the volume for melilitites, with wt % (MgO + FeO*) reaching ~45. Melilitites and kimberlites are well separated from the miscibility gap at both 1 and 2·5 GPa. The range of carbonatite compositions according to Woolley & Kempe (1989) was illustrated in this tetrahedron by Lee & Wyllie (1997*a*). Calcio-carbonatites and dolomitic carbonatites are clustered along the edge from CaO to the dolomite composition, extending a few percent toward the SiO_2 corner. Gold

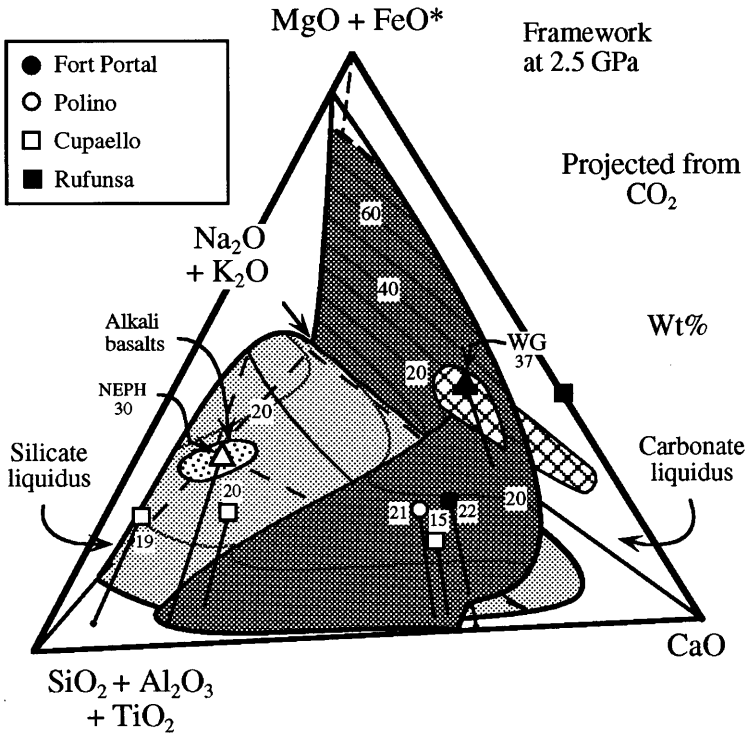

Fig. 7. Comparison of natural rock compositions and the generalized pseudoquaternary phase diagram at 2·5 GPa (compare Fig. 6), showing compositions of the selected effusive carbonatites at Rufunsa, Fort Portal, Polino and Cupaello (see text for sources of data). Numbers labeled for the rocks indicate wt % (MgO + FeO*). The partly schematic phase diagram is based on Wyllie & Huang (1976*a*), Baker & Wyllie (1990), and Lee & Wyllie (1996, 1997*a*). The silicate rocks (open squares '20' and '19') associated with the Cupaello carbonatite ('15') are also plotted. The cross-hatched volume including WG marks the range of experimental carbonatitic liquids from lherzolite, and is sketched to penetrate the silicate–carbonate field boundary surface. The dotted volume illustrates compositions of alkali basalts.

(1966) calculated that the average carbonatite contains 5·82 wt % SiO_2. Woolley & Kempe (1989) calculated average values (and ranges) for SiO_2 in calciocarbonatites and dolomitic carbonatites as 2·72 wt % (0–8·93 wt %) and 3·63 wt % (0·6–9·4 wt %), respectively, with total alkalis averaging <0·6 wt %. Natrocarbonatites have compositions near the mid-point of the edge CaO–(Na_2O + K_2O). Most carbonatite compositions lie well within the carbonate liquidus volume, separated from the silicate–carbonate liquidus surface at both 2·5 GPa (Fig. 7) and 1·0 GPa (Figs 8 and 9).

Experimental liquids from carbonated peridotites

The first liquids generated from carbonate peridotite must have compositions on the silicate–carbonate liquidus boundary surface. As noted above, the position of this surface varies with pressure (compare Figs 6 and 7 for 1 and 2·5 GPa). It has been established by experiments in model systems, whole-rock peridotites, and mixtures of minerals from peridotites that small-degree partial melting of carbonated peridotite at pressures greater than ~2 GPa produces dolomitic carbonatitic liquids with alkali contents varying according to the alkali content of the source material (e.g. Wyllie & Huang, 1975, 1976*a*; Wyllie, 1977; Eggler, 1978; Wyllie *et al.*, 1983; Wallace & Green, 1988; Thibault *et al.*, 1992; Dalton & Wood, 1993; Sweeney, 1994; Yaxley & Green, 1996).

Lee & Wyllie (1997*a*) reviewed the range of experimentally determined liquid compositions from dolomite–lherzolite in the tetrahedron framework, with particular reference to the alkali variations reported by Wallace & Green (1988; WG), Thibault *et al.* (1992), Dalton & Wood (1993), and Sweeney (1994). The liquids are shown in Fig. 7 by the cross-hatched volume which penetrates the estimated 2·5 GPa silicate–carbonate liquidus boundary surface. It extends in both directions because of the differences in source rocks studied (e.g. alkalis), and the variable experimental P–T conditions which are grouped together. Point WG shows the dolomitic nature of most near-solidus liquids from lherzolite, which are situated not far from the boundary surface. The results of Dalton & Wood (1993) diverge from this surface, extending from the dolomitic melt composition at the right end of the cross-hatched volume to more

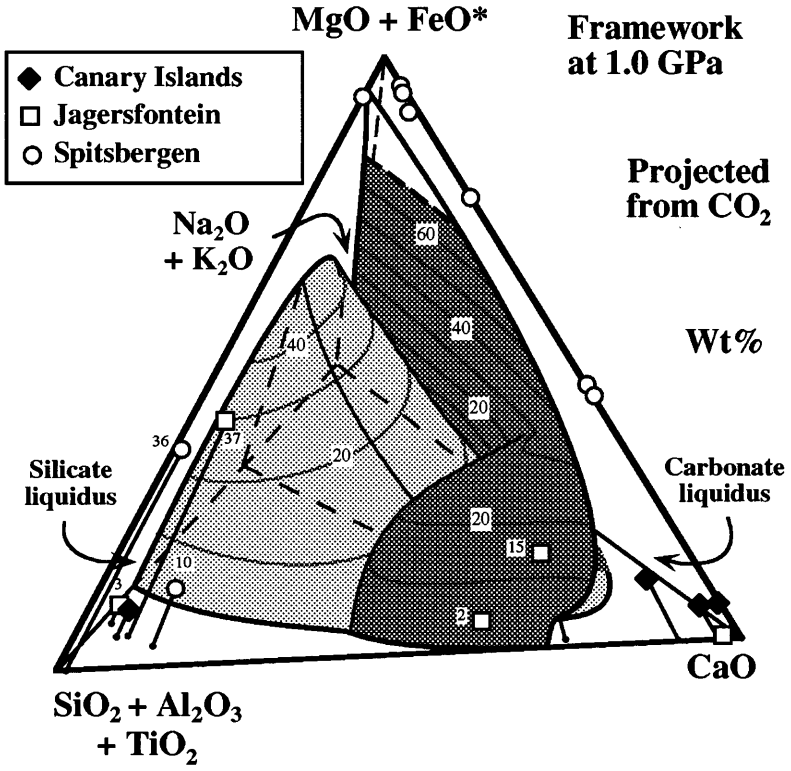

Fig. 8. Compositions of silicate glasses and carbonate globules in mantle xenoliths including Canary Islands harzburgite, Jagersfontein eclogite and Spitsbergen lherzolite (see text for sources of data). The framework is at 1·0 GPa, as in Fig. 6.

calcitic, alkali-poor compositions, with less SiO_2. The latter compositions were determined for a liquid coexisting with (magnesian calcite)-wehrlite, formed by successive reaction of lherzolite with the dolomitic liquid.

Yaxley & Green (1996) reported the compositions of sodic dolomitic carbonatite melts coexisting with lherzolite and with harzburgite, produced by reaction of CO_2 with wehrlite at 2·2 GPa. The low-temperature liquids (1050°C) project near the general area for near-solidus carbonatite melts in Fig. 7, with higher-temperature ones (1070°C) dissolving more silicate components, and therefore projecting into the primary silicate volume as expected.

Experimental data on silicate–carbonate liquid immiscibility at mantle conditions

The possibility that immiscible carbonatite liquids may be generated during normal melting processes in carbonated mantle appears to be precluded by the experiments of Baker & Wyllie (1990) and Lee & Wyllie (1997*a*), using bulk compositions which represent the compositional range of magmas expected in the upper subcontinental mantle. Baker & Wyllie (1990) determined at 2·5 GPa the position of the silicate–carbonate liquid miscibility gap intersected by mixtures of the primitive magnesian nephelinite NEPH (Figs 5 and 7) with selected carbonates. Lee & Wyllie (1997*a*) defined the equivalent miscibility gap at 1·0 GPa and 1200°C (Fig. 5).

The results showed that liquid paths between carbonatite liquid WG and silicate magmas (represented by primitive nephelinite NEPH and alkali basalts) were unlikely to intersect the miscibility gap. Baker & Wyllie (1990) used a triangular Hamilton projection; Lee & Wyllie (1997*a*) used the tetrahedron and isothermal curve A–A in Fig. 5. This conclusion is reinforced in the more complete tetrahedra of Figs 7 and 8. The progressive melting paths remain well above the entire range of the miscibility gap at both 2·5 GPa and 1·0 GPa.

Primary carbonatite melts from the mantle?

There is unambiguous experimental evidence that partial melting of mantle peridotite containing CO_2 would yield carbonate-rich liquid with major element composition corresponding to dolomitic magma (see above), through a range of pressures from ~2 GPa to at least 6 GPa (Dalton & Presnall, 1995, 1996). There are rare examples of mantle carbonates preserved in peridotite xenoliths

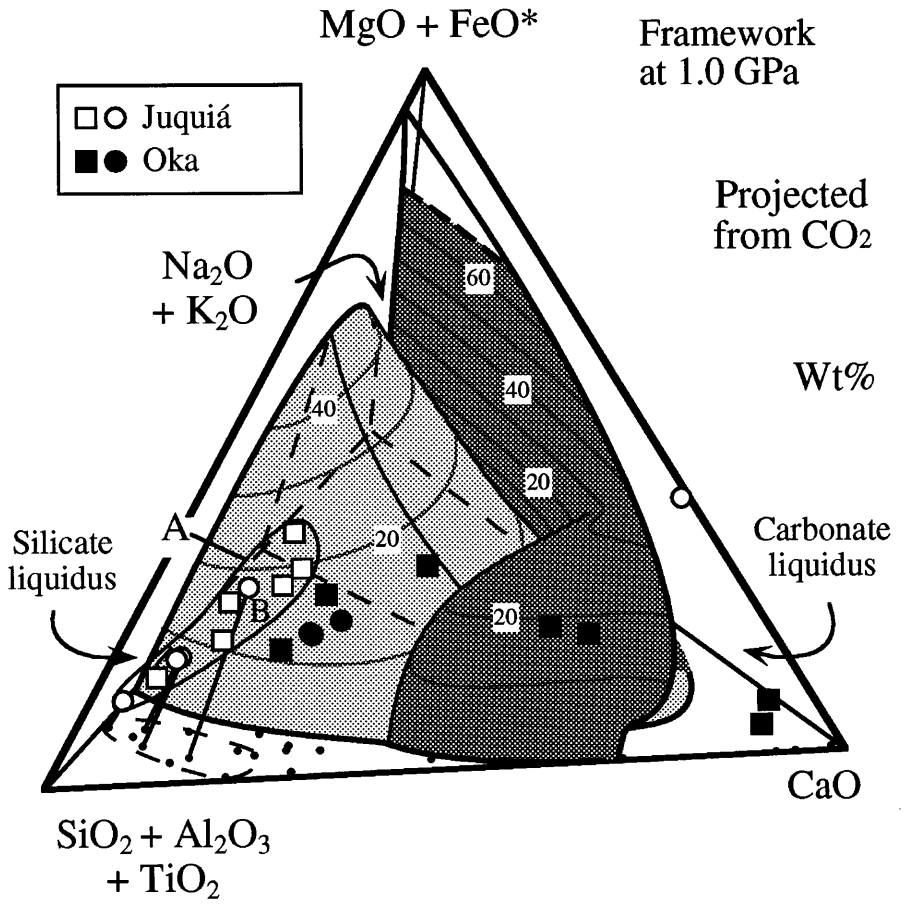

Fig. 9. Bulk compositions of cumulates and fine-grained rocks from Juquiá (in envelope A) and from Oka carbonatite complexes (see text for sources of data). Point B indicates a basanitic rock interpreted as the most primitive magma of the series A. The framework is at 1·0 GPa.

(e.g. Ionov *et al.*, 1996). There is metasomatic evidence for the reaction of mantle rocks with a carbonate-rich melt. There have been recent proposals based on petrology and field relationships that carbonate-rich melts from the mantle may reach the surface as primary magmas (e.g. Bailey, 1993; Barker, 1996*b*), or precipitate dolomitic carbonatites in the crust (Harmer & Gittins, 1997).

Ionov *et al.* (1996) described in detail the carbonates of mantle origin found in xenoliths from basalts in Spitsbergen, and reviewed the few previously reported occurrences of carbonates in mantle rocks. Their rarity in peridotite xenoliths is attributed to explosive decomposition of carbonates during transport to the surface (Eggler, 1975; Wyllie, 1978; Wyllie *et al.*, 1983; Canil, 1990). Recent reports of calcite ocelli in mantle xenoliths, which have been explained in terms of liquid immiscibility, are discussed below.

Carbonate-rich melts have been called upon to explain the metasomatic events observed in many mantle xenoliths (Green & Wallace, 1988; Yaxley *et al.*, 1991; Hauri *et al.*, 1993; Ionov *et al.*, 1993; Rudnick *et al.*, 1993). This proposal is largely based on the fact that some mantle rocks show extreme large ion lithophile element (LILE) enrichment patterns mimicking the geochemical signature of carbonatite melts. Very commonly there also exist within the peridotite host small patches of secondary olivine and clinopyroxene inclusions which are considered to be a reaction product between peridotite and carbonate-rich melts. The occurrence of such a reaction with decreasing pressure (i.e. during uprise of dolomitic magma) is shown by phase relationships (Wyllie & Huang, 1976*a*; Eggler, 1978), and by experiments showing that lherzolite and harzburgite can be converted to wehrlite by dolomitic carbonatitic liquids at crustal pressures (Wallace & Green, 1988; Dalton & Wood, 1993).

Keller (1981, 1989) presented evidence for effusive carbonatite magmas and concluded that primary crystallization in most carbonatite eruptives is dominated by calcite, despite the fact that the only observed carbonatite lava flow is the natrocarbonatite at Oldoinyo Lengai. Bailey (1993) summarized the occurrences of effusive

carbonatites, noting that mantle debris was generally carried in those which had minor or no association with silicate rocks. He suggested that these carbonatites formed from primary magmas derived directly from the mantle without much modification. Barker (1996*b*) supported the hypothesis of direct mantle origin for these extrusive carbonatites, modifying his previous conclusion that most carbonatites were derivatives from associated alkaline igneous rocks (Barker, 1989).

Of the carbonatite compositions listed by Bailey (1993) and Barker (1996*b*), those with high Fe/Mg ratios and low *mg*-numbers [molecular Mg/(Mg + Fe)], are unlikely candidates for primary mantle magmas. Bailey (1993) also interpreted some of the effusive carbonatites as differentiated products. Apart from these, there are only four effusive carbonatites designated as primary mantle magmas for comparison with the phase relationships in Fig. 7 at 2·5 GPa: (1) a dolomite droplet analysis from dolomitic carbonatite of Rufunsa (Bailey, 1989), and average calciocarbonatite compositions from (2) Fort Portal (Barker & Nixon, 1989), (3) Polino (Stoppa & Lupini, 1993), and (4) Cupaello (Stoppa & Cundari, 1995).

The dolomite from Rufunsa (filled square, Fig. 7) plots directly on the CaO–(MgO + FeO*) edge of the tetrahedron, clearly separated from the liquid compositions coexisting with carbonated lherzolite (cross-hatched area). Despite its 'droplet' shape, the dolomite composition and the carbonate phase diagram (Irving & Wyllie, 1975; Byrnes & Wyllie, 1981) preclude it from being an original liquid. However, it could represent a mineral precipitated from a dolomitic mantle melt such as WG.

Three calciocarbonatites (Fort Portal, Polino, and Cupaello) in Fig. 7 contain high SiO_2 (~15–19 wt %), with (MgO + FeO*) ranging from 10 to 16 wt % (15–22 wt % volatile-free). The rocks project within the primary silicate volume, but near the silicate–carbonate boundary surface (compare the numbers for the rocks and the contours on the surface). The Fort Portal carbonatites contain as much as 15% xenocrysts and basement xenoliths (Barker & Nixon, 1989), so a correction for silicate contamination would move the composition of the rock even closer to the surface. The proximity of the effusive rock compositions to the silicate–carbonate boundary surface is consistent with an origin of the magmas by partial melting of a carbonated silicate rock, but the calciocarbonatite compositions do not correspond to any liquid which could be derived by equilibrium partial melting of any standard mantle peridotite. With decreasing pressure to 1·0 GPa (Fig. 8), the silicate–carbonate liquidus boundary surface moves further from the projected carbonatites in Fig. 7, indicating that if these were magmas generated from carbonated silicate rocks near the Moho, partial melting must have progressed from the carbonate–silicate assemblage on the boundary surface to higher temperatures through the silicate liquidus volume.

The Cupaello carbonatite tuff is associated with melilitite pyroclastic breccia. Stoppa & Cundari (1995) concluded on the basis of their field study that the suite provides direct evidence for immiscibility of carbonatite magma from 'kamafugite' (melilitite) magma. The analyses of a silicate fragment and its matrix (Stoppa & Lavecchia, 1992) are shown in Fig. 7 (open squares '20' and '19'). Both silicate data points and the associated carbonatite composition (square '15') plot far away from the miscibility gap at 2·5 GPa and at 1·0 GPa (Fig. 8), so evidence in our experimental framework denies the liquid immiscibility interpretation for the mantle and deep crust. An explanation for these may be found in experiments with melilitite compositions at crustal pressures (e.g. Kjarsgaard & Hamilton, 1989*b*; Kjarsgaard, 1997).

The experimental evidence demonstrates that primary mantle-derived carbonatite magmas are possible. According to the phase relationships summarized in Figs 7 and 8, the carbonatite rocks which have been proposed as primary magmas bear no relationship to the magma compositions expected from small degree partial melting of CO_2-bearing mantle peridotites at pressures between 2 GPa (Lee & Wyllie, 1997*a*) and 6 GPa (Dalton & Presnall, 1995, 1996). Nor do they match the more calcic experimental liquids reported by Dalton & Wood (1993) from repeated reactions between carbonatite melts and wehrlite. The occurrence of primary carbonatite magmas remains an appealing prospect, but current evidence requires that such magmas (liquids) should have compositions within the cross-hatched volume in Fig. 7, commonly closer to WG than to those richer in Ca/Mg. We agree with Eggler (1989) that primary mantle carbonatites should occur in isolation, as do kimberlites.

Carbonate ocelli in mantle xenoliths: liquid immiscibility?

There have been several reports of rounded calcites, commonly termed ocelli, in upper-mantle peridotite and eclogite xenoliths (e.g. Amundsen, 1987; Ionov *et al.*, 1993; Pyle & Haggerty, 1994; Kogarko *et al.*, 1995). The ocelli are generally associated with metasomatic events, and are adjacent to silicate glasses of various compositions. The textures, as reviewed below, have been interpreted as products of liquid immiscibility between silicate and carbonate liquids. The phase relationships indicate that none of these carbonate compositions can represent equilibrium immiscible liquids—they are too far removed from the miscibility gap, well inside the 'forbidden volumes' of the primary carbonate liquidus.

In Fig. 8 the compositions of the proposed immiscible carbonate liquids are compared with the associated silicate glasses within the 1·0 GPa phase diagram framework representing the conditions for the uppermost mantle. Their positions with respect to the somewhat changed phase boundary surfaces at greater depths can be visualized in Fig. 7 (2·5 GPa).

Kogarko *et al.* (1995) described carbonate globules in harzburgite nodules from the Canary Islands, with compositions given by the filled diamonds near the CaO corner of Fig. 8. The carbonates are magnesian calcites, with very low alkali contents. The measured SiO_2 contents might result from minor silicate inclusions in the carbonates; one analysis does show zero SiO_2. The representative silicate glass plots well within the primary silicate volume (filled diamond, near the silicate corner), about 10 wt % alkalis outside the corresponding miscibility contour curve, at 5 wt % (MgO + FeO*). The compositions of calcite ocelli and silicate glass thus bear no relationship to the experimentally determined miscibility gap, and some other explanation is needed.

In another Canary Island study, Frezzotti *et al.* (1994) analyzed silicate glass and carbonate spherules in dunite xenoliths, noting the difficulty in analyzing small inclusions. They showed carbonate compositions corresponding to magnesian calcite and dolomite with up to 4 wt % SiO_2, and (Si,Mg,Fe)-glass compositions with some volatile components, and suggested that they were related by liquid immiscibility. The two sets of alkali-free phases project, respectively, on the CaO–(MgO + FeO*) axis, or the (MgO + FeO*)–(SiO_2 + Al_2O_3 + TiO_2) axis, and tie-lines between them would pass nowhere near the silicate–carbonate miscibility gap in Figs 8 and 7, respectively.

Pyle & Haggerty (1994) presented a detailed study of silicate glasses containing calcite ocelli in eclogite xenoliths from the Jagersfontein kimberlite. The carbonate ocelli have compositions very near pure calcite, as shown by the open square in Fig. 8. Two types of glasses were found, as shown by the open squares in the silicate liquidus volume in Fig. 8. The Na–Al-rich silicate glass near the SiO_2 corner ('3', referred to as sodic glass, of jadeite affinity) contains low Ca, Mg and Fe, similar to the glasses of the Canary Islands harzburgite nodules. The Mg-rich silicate glass ('37', referred to as potassic glass, of phlogopite affinity), is also Ca poor, with the major alkali component being potassium. Pyle & Haggerty (1994) proposed a model involving decompressive melting of alkali-bearing phases in the eclogite, combined with injection and through-flushing of a CO_2–H_2O-rich fluid or melt to form two immiscible liquids; a Ca-rich carbonatite liquid, and a conjugate alkali-rich silicate liquid. It is clear in Fig. 8 that the alkali contents of the glasses and calcite ocelli are too low for a tie-line between them to intersect the miscibility gap, and the distance between tie-line and miscibility gap is even greater at the higher pressure of Fig. 7. Pyle & Haggerty (1994) estimated the parental liquid compositions for each unmixed pair, liquids '2' and '15' corresponding to the parent magmas which generated the sodic liquid '3' and the potassic affinity liquid '37', respectively. These estimated parental liquids plot very close to the silicate–calcite liquidus surface (Fig. 8). Perhaps the parental liquids precipitated both calcite and silicate minerals (mainly natrolite and phlogopite, respectively) after infiltration into the ecolgites. Upon uprise, decompressive melting of some portions of the alkali-bearing silicate minerals might have produced the sodic and potassic glasses.

Globules of nearly pure calcite in silicate glasses were also reported by Seifert & Thomas (1995), who studied melt inclusions in olivine melilitite and wehrlite xenoliths of the Elbe zone, Germany. Their silicate glass is similar in composition to that reported by Kogarko *et al.* (1995; black diamond, Fig. 8). They proposed that the calcite globules represented immiscible carbonate liquids, but as in the other examples, a tie-line between the glass and the calcite would not intersect the liquid miscibility gap at any pressure, and there is no experimental evidence to support the occurrence of liquid immiscibility in these examples.

Examples of carbonate ocelli from Spitsbergen occupy a different composition range (Amundsen, 1987; Ionov *et al.*, 1993). Round carbonates near dolomite, ankerite or magnesite in composition, with very low alkali contents (open circles in Fig. 8), coexist with two glasses. One glass is ultramafic (open circle '36', Fig. 8), and the other is basaltic (Na–Al-rich silicate, open circle '10'). The ultramafic glass contains nearly no alkalis, whereas the basaltic glass plots near the sodic glass of Pyle & Haggerty (1994), but contains higher (CaO + MgO + FeO*). Amundsen (1987) proposed three-liquid immiscibility to account for these three phases. Ionov *et al.* (1993) proposed a more elaborate process, involving decomposition and melting of primary dolomite and the generation of coexisting immiscible Na–Al-rich silicate liquid and carbonate-rich silicate-bearing liquid, which subsequently separated into Mg-rich silicate glass and carbonate. All three compositions are located well outside the miscibility gap, so the phase relationships indicate that neither of these immiscible processes could occur. Ionov *et al.* (1996) later concluded that both dolomite and magnesian calcite were primary, and suggested that the amorphous magnesite–ankerite was formed as a result of melting and breakdown of primary carbonates; the Mg-rich glass may have been formed by decompression-induced dissolution of olivine into a pre-existing carbonate-rich melt.

The location of these specific examples of rounded carbonates and coexisting silicate glasses in mantle

samples in Fig. 8 is consistent with the previous conclusions of Baker & Wyllie (1990) and Lee & Wyllie (1997*a*) that silicate–carbonate liquid immiscibility is unlikely to be encountered during mantle melting processes. The carbonate-rich compositions are in the forbidden volume for derivative liquids. Lee *et al.* (1994) and Lee & Wyllie (1996, 1997*a*) demonstrated that through a wide range of compositions, similarly rounded calcite grains coexisting with silicate or silicate–carbonate liquids were in fact crystalline calcite at experimental conditions, and not immiscible liquids. Rounded carbonate crystals have been produced experimentally in many carbonate and silicate–carbonate systems (e.g. calcite—Wyllie & Tuttle, 1960; Cooper *et al.*, 1975; Huang *et al.*, 1980; Lee *et al.*, 1994; magnesite—J. Dalton, personal communication, 1995), and round gregoryite has been described from Oldoinyo Lengai lavas (Cooper *et al.*, 1975; Church & Jones, 1995). Lee & Wyllie (1996) therefore concluded that the evidence for the formation of immiscible liquids with ~99 wt % $CaCO_3$ (round calcites) previously reported (Kjarsgaard & Hamilton, 1988, 1989*a*; Brooker & Hamilton, 1990) was invalid (confirmed later by B. A. Kjarsgaard, personal communication, 1994, reinterpretation in fig. 5 of Macdonald *et al.*, 1993). Figure 8 reinforces the conclusion, showing that at least the calcite–dolomite range of carbonates is clearly separated from the miscibility gap at 1·0 GPa.

Primary silicate magmas and crustal carbonatite magmas

Gittins (1989) addressed the dichotomy 'between those who saw carbonatites as developing essentially within the crust, or only slightly below it, by modification of a mantle-derived magma and those who emphasized the vexed question of a kimberlite–carbonatite association and took a quantum leap into the bowels of the earth to seek the birthplace of carbonatites'. The evidence from isotopes now points unambiguously to a mantle source for carbonatites or their parent magmas (Deines, 1989; Bell & Blenkinsop, 1989; Kwon *et al.*, 1989), with indications that they are derived from two mantle reservoirs, but isotopic data do not permit distinction among the three processes currently favored for their origin:

(1) primary magmas from the mantle,

(2) fractional crystallization of a carbonated primary silicate magma, or

(3) separation of an immiscible carbonatite magma from a primary or evolved silicate parent.

We have concluded above that the compositions of effusive carbonatites so far identified as primary magmas from the mantle do not satisfy the available phase equilibrium data. However, experimental evidence confirms that primary magmas of dolomitic compositions are possible, and several dolomitic carbonatites in Africa have recently been proposed on the basis of petrological, geochemical and field evidence as derived from primary magmas (Harmer & Gittins, 1997). We now examine processes (2) and (3). Petrologists have long appealed to some kind of 'carbonated alkali peridotite magma' as the parent of carbonatite magmas (e.g. King & Sutherland, 1960), and more recently magmas such as olivine nephelinites, melilitites, and evolved nephelinites, phonolites, ijolites and syenites have been specified in the processes leading to fractionated or immiscible carbonatite magmas. Variations on these themes are legion, and they are well represented in the detailed schemes of Le Bas (1977, figs 24.1 and 24.2; 1989) and Kjarsgaard *et al.* (1995, fig. 9).

Gittins (1989) rejected process (2) in favor of a primary mantle carbonatite magma (1) partly because the existence of a 'carbonated nephelinite' rich in dissolved CO_2 remains speculative. Wyllie & Huang (1975, 1976*b*) showed, however, that progressive melting of a mantle peridotite which yields a carbonatite liquid next produces 'kimberlitic' magma, or 'high-alkali, low-SiO_2 carbonated magma' (depending on conditions such as pressure), which corresponds closely to some of the proposed mantle parent magmas. The progression from dolomitic carbonatite liquid to kimberlite-like liquid has been confirmed experimentally at 6·0 GPa by Dalton & Presnall (1996). If primary mantle carbonatites are possible, then so are primary carbonated olivine nephelinites or melilitites (Wendlandt and Eggler, 1980*a*, 1980*b*).

Lee & Wyllie (1996, 1997*b*) illustrated various crystallization paths for silicate–CO_2 liquids in the system Na_2O–CaO–Al_2O_3–SiO_2–CO_2, with the field boundaries outlined in Fig. 1. Depending on the initial composition and P–T condition, the cooling liquids may reach the miscibility gap, or follow a path to the silicate–carbonate coprecipitation boundary, or solidify completely to silicates with evolution of CO_2 vapor. Both fractional crystallization and liquid immiscibility may be important in the genesis of subvolcanic and volcanic carbonatites, and the question is to define the most probable path for a particular occurrence based on integrated evidence from field, geochemical and experimental studies.

Figure 7 confirms that a primitive magnesian nephelinite and the alkali basalt field are far removed from the miscibility gap at 2·5 GPa, and the same is true for 1·0 GPa (Fig. 9). Figure 9 shows a differentiation trend for a suite of rocks from the alkaline carbonatite complex of Juquiá, São Paulo (Beccaluva *et al.*, 1992). The most primitive liquid is basanitic, marked by B, with 25 wt % (MgO + FeO*), which is distant from the miscibility gap shown at both 2·5 GPa (Fig. 7) and 1·0 GPa (Fig. 9). The bulk compositions of silicate rocks representing both magmas (open circles) and cumulates (open squares) are plotted in volume A. The data define a trend within the

silicate volume from the primitive mafic rocks to the more evolved nepheline syenites. The trend approaches the miscibility gap for 1·0 GPa as (MgO + FeO*) decreases, but does not quite reach it. Many East African carbonatite complexes show a composition series of silicate rocks similar to this trend [see data compiled by Le Bas (1977)], and experimental data confirm the probability that these evolved magmas can reach the miscibility gap (Kjarsgaard & Peterson, 1991). On the basis of field observations and geochemical data, Beccaluva *et al.* (1992) concluded that the dolomitic carbonatite (open circle, carbonate side, Fig. 9) in the Juquiá complex was a calcite-fractionation product of a calciocarbonatite magma separated from a CO_2-rich nepheline syenite parent by liquid immiscibility. We conclude that although the dolomitic carbonatite composition (Ca/Mg) is consistent with fractionation of a more calcic parent (Byrnes & Wyllie, 1981), it cannot represent a liquid magma because it lies within the forbidden carbonate volume, too far from the silicate–carbonate liquidus boundary.

A different trend is shown by the silicate and carbonatite rocks from the Oka complex. Figure 9 shows rock compositions from Oka tabulated by Treiman & Essene (1985): fine-grained rocks (filled circles) represent liquids, and coarse-grained (filled squares) represent cumulates. These rock compositions lie in a trend extending from the primary silicate volume to the calcite corner. Treiman & Essene (1985) proposed that the Oka rocks formed from immiscible silicate and carbonatite magmas *in situ*. We conclude that the occurrence of immiscibility is precluded, because all of the listed compositions plot well outside of the 1·0 GPa (and 2·5 GPa, Fig. 7) miscibility gap. According to the phase relationships at this pressure, the sequence of rocks could be derived by process (2). A parent, CO_2-bearing silicate liquid with composition near the filled circles could follow a path toward the silicate–carbonate liquidus coprecipitation surface, where the silicate minerals would be joined by calcite. The silicate–calcite rocks of Oka could be generated as the evolving liquid followed a path on the cotectic surface. The liquid thus becomes more alkalic and less siliceous (the boundary is more carbonate rich at the alkalic portion of the tetrahedron; compare the analogous boundary e–fg in Fig. 2c), and thus becomes capable of precipitating carbonatitic rocks with higher carbonate to silicate ratios, as indicated by the most calcite-rich rocks in Fig. 9. Watkinson & Wyllie (1971) and Lee & Wyllie (1994) previously demonstrated, from experimental results in a different model system, that fractional crystallization of a carbonated nepheline-normative liquid could yield, by fractionation, a sequence of mineral assemblages corresponding to the silicate–carbonatite sequence developed at Oka.

Process (3) involving liquid immiscibility in the crust is currently favored by many petrologists. Indirect evidence is provided by the observation that fractionation paths of primary magmas similar to that for the Juquiá sequence in Fig. 9 bring evolved nepheline-normative magmas close to the low (MgO + FeO*) miscibility gap in Figs 7 and 9 (Kjarsgaard & Hamilton, 1989*a*). Direct evidence is given by petrographic observations of rocks at Shombole volcano and at Oldoinyo Lengai, and confirmed by experiments (e.g. Kjarsgaard & Peterson, 1991; Kjarsgaard *et al.*, 1995).

There is convincing evidence for liquid immiscibility between the silicate magmas and the Oldoinyo Lengai natrocarbonatite (e.g. Dawson *et al.*, 1994, 1996; Church & Jones, 1995; Kjarsgaard *et al.*, 1995; Peterson & Kjarsgaard, 1995). Current interpretations for the origin of the Oldoinyo Lengai lavas involve a primary olivine melilitite from the mantle. This evolves by differentiation within the crust to wollastonite nephelinites capable of exsolving alkali-rich carbonatite liquids (e.g. Church & Jones, 1995; Peterson & Kjarsgaard, 1995; Dawson *et al.*, 1996). Kjarsgaard *et al.* (1995) conducted experiments at low pressures and moderate temperatures to reproduce the conditions operating to generate the immiscible Oldoinyo Lengai lavas. They demonstrated the significance of peralkalinity, the complex relationships related to amount of CO_2, and the large variations in geometry of the miscibility gap occurring at low pressures (Koster van Groos & Wyllie, 1966).

Kjarsgaard & Peterson (1991) described calcite-rich globules with distinctive quench texture, representing immiscible calciocarbonatite liquids in Shombole lavas. The compositions of the lavas project to the general area for evolved alkalic rocks as in Fig. 9 (lower portion of volume A). Kjarsgaard & Peterson (1991) suggested that the carbonatite liquids require a nephelinite parent less peralkaline than that of the natrocarbonatite. They confirmed experimentally that Shombole rocks $\pm$ added calcite could produce immiscible silicate-rich liquids of low peralkalinity, and carbonatite liquids with much higher $CaCO_3$ and lower alkali contents than the compositions of natrocarbonatites. These liquids project near the (MgO + FeO*)-poor, low alkalic region of the miscibility gap surface in Fig. 9 [as shown in fig. 3 of Hamilton & Kjarsgaard (1993)]. Hamilton & Kjarsgaard (1993) further reported an immiscible carbonatite liquid with 90 wt % $CaCO_3$ when plotted in terms of carbonate components only, but when the presence of silicate components is taken into account, they plotted the same point in a Hamilton projection which corresponds to a composition with ~75 wt % $CaCO_3$, consistent with the miscibility gaps in Figs 1 and 7–9, and given by Macdonald *et al.* (1993).

The composition of an immiscible carbonatite magma depends on many factors, including the peralkalinity of

the silicate magma. Comparison of rock compositions with the pseudoquaternary phase relationships in Figs 7–9 suggests that many evolving silicate magmas are likely to intersect the miscibility gap only when they have low (MgO + FeO*); the immiscible carbonatite magma would also be low in (MgO + FeO*), and rich in calcite and alkali carbonates (see field boundary g–n in Fig. 1). [However, see Kjarsgaard & Hamilton (1989*b*) and Kjarsgaard (1997) for divergent results with melilititic compositions.] Lee & Wyllie (1996, 1997*b*) presented a detailed evaluation of immiscibility relationships using model systems such as Fig. 1. The ratio of CaO/(Na_2O + K_2O) in the silicate magma when it reaches the field boundary f–m (Figs 1 and 2a) defines the ratio in the immiscible carbonatite magma (field boundary g–n in Figs 1 and 2a), according to the array of tie-lines between f–g and m–n. Lee & Wyllie (1997*b*) concluded that immiscible carbonatite magmas would tend to cluster in the area near g of Fig. 1, with ~75–80 wt % $CaCO_3$ and ~15 wt % Na_2CO_3.

The immiscible carbonatite magma does not precipitate carbonates (except for limiting compositions such as g in Fig. 1, which is represented by the field boundary for the curve of intersection of the two surfaces in Figs 6–9) until it has been physically separated from the consolute silicate liquid; then it cools through some temperature interval precipitating only silicates until it reaches the silicate–carbonate field boundary, e.g. g–o in Figs 1 and 2a, or the shaded silicate–carbonate liquidus boundary surface in Figs 7–9.

SUMMARY OF SPECIFIC POSSIBILITIES AND IMPOSSIBILITIES IN CARBONATITE PETROGENESIS

The examples above have illustrated where various rocks and rock suites plot within the phase elements which we have constructed, permitting specific conclusions about the possibility or impossibility of the proposed processes for these occurrences. There are many paths through the tetrahedron, and the distribution of phase elements within it at various pressures (and for varied compositions) places constraints on processes. We emphasize that similar end products may be formed via different processes, and make no attempt to formulate a general petrogenetic scheme for the origin of carbonatites. What we offer below is a series of more general signposts of what is permitted or denied at various stages during solidification of a silicate–CO_2 parent magma (mainly within the mantle and deep crust, but with some remaining valid at lower-crustal pressures). We have not attempted to fill in gaps with speculation or evidence from sources other than phase equilibrium. On the basis of experimental evidence discussed and cited above, we consider that the following conclusions should be applied to any comprehensive petrogenetic scheme which is based on field evidence, petrology, and geochemistry.

(1) Parental magmas of carbonatites are mantle derived, and must be CO_2 enriched ('carbonated').

(2) The pseudoquaternary system CaO–(MgO + FeO*)–(Na_2O + K_2O)–(SiO_2 + Al_2O_3 + TiO_2) with CO_2 provides a framework for evaluating possible magmatic processes. The three key features are: (a) the liquidus surface enclosing the volume of silicate–carbonate liquid immiscibility, (b) the silicate–carbonate liquidus surface for the coprecipitation of silicates and carbonates, and (c) the curve of intersection between these two surfaces, defining conditions for the coexistence of two immiscible liquids, silicate, and calcite. The relationship between the surfaces, which varies as a function of pressure and magma composition (especially Mg/Ca, Ca/Na, Al/Si), controls the nature of carbonate-rich magmas derived from parent silicate magmas.

(3) Experimentally determined phase boundaries in the system indicate that immiscible carbonatite magmas contain no more than ~80 wt % $CaCO_3$, and at least ~10 wt % $(Na,K)_2CO_3$.

(4) The carbonate content of magmas derived from silicate parents is limited by the position of the silicate–carbonate liquidus surface. The liquidus volume for primary carbonate precipitation is thus a 'forbidden volume' for such magmas. This appears to limit the compositions of carbonatite magmas to less than ~85 wt % $CaCO_3$.

(5) Carbonate minerals occur in mantle rocks, but those in contact with the silicate assemblage in the peridotite host should decompose during even rapid transit to the surface.

(6) Carbonate-rich magmas may be generated at depths greater than ~70 km by partial melting of carbonated (dolomite–magnesite) peridotite. The near-solidus magmas lie on the silicate–carbonate liquidus field boundary, with compositions dominated by the liquidus of the system $CaCO_3$–$MgCO_3$, and with minor variations in Ca/Mg and alkali contents reflecting directly the peridotite mineralogy. Liquid compositions are dolomitic, with Ca/(Ca + Mg) ~0·5–0·7 from 2 GPa to at least 6 GPa (depth 200 km). Even when the subsolidus carbonate changes from dolomite to magnesite with increasing pressure, the liquid composition remains dolomitic. Carbonatite magmas in the mantle are the first (lowest-temperature) part of a continuum of small-volume partial melts including melilitites and kimberlites.

(7) The phase relationships show that the formation of (equilibrium) carbonate-rich liquids immiscible with primitive silicate magmas in the mantle is unlikely, which denies both the formation of immiscible $CaCO_3$ ocelli

and the generation of primary natrocarbonatite magmas in the subcontinental mantle.

(8) Claims for primary calciocarbonatite magmas remain without experimental support. Primary carbonatite magmas from the mantle should have compositions dominated by calcic dolomite. Their intrusive style should approximate that of kimberlites, and they should tend to be isolated, and not directly associated with large volumes of alkaline igneous rocks.

(9) Rising carbonate-rich magmas retaining equilibrium with mantle will react, crystallize and release CO_2 vapor at depths of ~70 km, with the metasomatic transformation of lherzolite toward wehrlite. At shallower depths, wehrlite (but no other peridotite) can coexist with carbonatite magma relatively enriched in Ca/Mg.

(10) Most carbonatite magmas are derived from carbonated silicate parents, which could follow one of three kinds of crystallization paths: (a) to a liquidus–solidus terminal point where they precipitate silicates and evolve CO_2 vapor, (b) to a silicate–carbonate field boundary where silicates and carbonates are coprecipitated, or (c) to a miscibility gap field boundary where a carbonate-rich magma is exsolved, without the coprecipitation of calcite except along the limiting field boundary where the two major liquidus surfaces intersect.

(11) Immiscible carbonate-rich liquids separated from liquids corresponding to many natural silicate magmas tend to be concentrated near calciocarbonatite compositions, with the maximum $CaCO_3$ being ~75–80 wt %, and $(Na,K)_2CO_3$ contents near 15 wt %. [Compare the range with the compositional limit of immiscible carbonatite magmas (3), and the limit of the silicate–carbonate liquidus surface (4).] Some silicate parents (e.g. with higher Na/Ca) may yield immiscible natrocarbonatite liquids.

(12) The separation of some immiscible carbonate-rich liquids is accompanied by precipitation of calcite [see (10c)], but the greater range of immiscible liquids do not precipitate carbonates while they coexist with silicate parents. Only after the carbonate-rich liquid is physically separated from the parent liquid, and cooled with the precipitation of silicates, does it reach the silicate–carbonate field boundary.

(13) Carbonatites with compositions within the forbidden carbonate liquidus volume cannot represent original liquid magma compositions—they must represent cumulates.

(14) Carbonate-rich magmas precipitate carbonatite rocks (cumulates) only when they reach the silicate–carbonate liquidus field boundary. Some parent magmas may reach this boundary by direct crystallization without immiscibility, but most traverse the miscibility gap. Along the field boundary, the coprecipitation of calcite inevitably drives the residual liquid toward more alkali-rich compositions (natrocarbonatites).

(15) From (11) and (14), two ways to make alkali-rich carbonatite liquids are possible.

(16) There appear to be no reasonable paths of crystallization, with or without a vapor, which would generate residual calciocarbonatite magmas from a high-temperature immiscible natrocarbonatite magma.

(17) The available experimental data indicate that the compositions of dolomitic carbonatites are so far removed from the miscibility gap that they cannot be produced as immiscible liquids from silicate parent magmas. Dolomitic carbonatite magmas may be generated by fractionation of calciocarbonatite magmas (on the basis of liquidus phase relationships in $CaCO_3$–$MgCO_3$), or as primary magmas.

(18) The effect of volatile components H_2O and F on these processes needs more detailed evaluation, but the evidence available suggests that in expected natural concentrations they will not change significantly the topological relationships near the liquidus, and therefore would not change the generality of the conclusions outlined above. Liquidus temperatures would be slightly lowered, but solidus temperatures could be greatly lowered. The presence of these components in higher concentrations in residual liquids at lower temperatures may introduce different crystallization paths. At very low subvolcanic pressures, changes in phase geometry may modify the liquidus paths.

(19) The effects of supercooling and quench crystallization in carbonate-rich liquids require that caution be exercised in the interpretation of the products of rapid volcanic processes, or of small-scale features and textures.

ACKNOWLEDGEMENTS

We thank J. Gittins, B. A. Kjarsgaard, and A. P. Jones for helpful comments. This research was supported by the Earth Science section of the US National Science Foundation, Grant EAR-921886. This is Contribution 8505 of the Division of Geological and Planetary Sciences, California Institute of Technology.

REFERENCES

Amundsen, H. E. F. (1987). Evidence for liquid immiscibility in the upper mantle. *Nature* **327,** 692–695.

Bailey, D. K. (1989). Carbonate melt from the mantle in the volcanoes of south-east Zambia. *Nature* **338,** 415–418.

Bailey, D. K. (1993). Carbonate magmas. *Journal of the Geological Society, London* **150,** 637–651.

Baker, M. B. & Wyllie, P. J. (1990). Liquid immiscibility in a nephelinite–carbonate system at 25 kbars and implications for carbonatite origin. *Nature* **346,** 168–170.

Barker, D. S. (1989). Field relations of carbonatites. In: Bell, K. (ed.) *Carbonatites: Genesis and Evolution*. London: Unwin Hyman, pp. 38–69.

Barker, D. S. (1996*a*). Consequences of recycled carbon in carbonatites. *Canadian Mineralogist* **34,** 373–387.

Barker, D. S. (1996*b*). Carbonatite volcanism. In: Mitchell, R. H. (ed.) *Undersaturated Alkaline Rocks: Mineralogy, Petrogenesis, and Economic Potential. Mineralogical Association of Canada, Short Course* **24,** 45–61.

Barker, D. S. & Nixon, P. H. (1989). High-Ca, low-alkali carbonatite volcanism at Fort Portal, Uganda. *Contributions to Mineralogy and Petrology* **103,** 166–177.

Beccaluva, L., Barbieri, M., Born, H., Brotzu, P., Coltorti, M., Conte, A., Garbarino, C., Gomes, C. B., Macciotta, G., Morbidelli, L., Ruberti, E., Siena, F. & Traversa, G. (1992). Fractional crystallization and liquid immiscibility processes in the alkaline-carbonatite complex of Juquiá (São Paulo, Brazil). *Journal of Petrology* **33,** 1371–1404.

Bell, K. (ed.) (1989). *Carbonatites; Genesis and Evolution*. London: Unwin Hyman.

Bell, K. & Blenkinsop, J. (1989). Neodymium and strontium isotope geochemistry of carbonatites. In: Bell, K. (ed.) *Carbonatites: Genesis and Evolution*. London: Unwin Hyman, pp. 278–300.

Bell, K. & Keller, J. (eds) (1995). *Carbonatite Volcanism: Oldoinyo Lengai and the Petrogenesis of Natrocarbonatites. IAVCEI Proceedings in Volcanology 4*. Berlin: Springer-Verlag.

Brey, G. (1978). Origin of olivine melilitites—chemical and experimental constraints. *Journal of Volcanology and Geothermal Research* **3,** 61–88.

Brooker, R. A. & Hamilton, D. L. (1990). Three-liquid immiscibility and the origin of carbonatites. *Nature* **346,** 459–462.

Brooker, R. & Holloway, J. R. (1997). The role of CO_2 saturation in silicate–carbonatite magmatic systems. *GAC–MAC Annual Meeting, Abstract Volume* A-18.

Byrnes, A. P. & Wyllie, P. J. (1981). Subsolidus and melting relations for the join $CaCO_3$–$MgCO_3$ at 10 kb. *Geochimica et Cosmochimica Acta* **45,** 321–328.

Canil, D. (1990). Experimental study bearing on the absence of carbonate in mantle-derived xenoliths. *Geology* **18,** 1011–1013.

Canil, D. & Scarfe, C. M. (1990). Phase relations in peridotite + CO_2 systems to 12 GPa: implications for the origin of kimberlite and carbonate stability in the Earth's upper mantle. *Journal of Geophysical Research* **95,** 15805–15816.

Church, A. A. & Jones, A. P. (1995). Silicate–carbonate immiscibility at Oldoinyo Lengai. *Journal of Petrology* **36,** 869–889.

Clague, D. A. & Frey, F. A. (1982). Petrology and trace-element geochemistry of the Honolulu volcanics, Oahu—implications for the oceanic mantle below Hawaii. *Journal of Petrology* **23,** 447–504.

Cooper, A. F., Gittins, J. & Tuttle, O. F. (1975). The system Na_2CO_3–K_2CO_3–$CaCO_3$ at 1 kilobar and its significance in carbonatite petrogenesis. *American Journal of Science* **275,** 534–560.

Dalton, J. A. & Presnall, D. C. (1995). Phase relations in the system CaO–MgO–Al_2O_3–SiO_2–CO_2 from 4·0 to 6·0 GPa with applications to the generation of kimberlites and carbonatites. *EOS Transactions, American Geophysical Union* **76,** 697.

Dalton, J. A. & Presnall, D. C. (1996). Melting of a model carbonated lherzolite in the system CaO–MgO–Al_2O_3–SiO_2–CO_2 at 6·0 GPa: the continuous transition between carbonatite and group 1B kimberlite magmas. *EOS Transactions, American Geophysical Union* **77,** 817.

Dalton, J. A. & Wood, B. J. (1993). The compositions of primary carbonate melts and their evolution through wallrock reaction in the mantle. *Earth and Planetary Science Letters* **119,** 511–525.

Dawson, J. B. & Hawthorne, J. B. (1973). Magmatic sedimentation and carbonatite differentiation in kimberlite sills at Benfontein, South Africa. *Journal of the Geological Society, London* **129,** 61–85.

Dawson, J. B., Pinkerton, H., Pyle, D. M. & Nyamweru, C. (1994). June 1993 eruption of Oldoinyo Lengai, Tanzania: exceptionally viscous and large carbonatite lava flows and evidence for coexisting silicate and carbonate magmas. *Geology* **22,** 799–802.

Dawson, J. B., Pyle, D. M. & Pinkerton, H. (1996). Evolution of natrocarbonatite from a wollastonite nephelinite parent: evidence from the June (1993) eruption of Oldoinyo Lengai, Tanzania. *Journal of Geology* **104,** 41–54.

Deines, P. (1989). Stable isotope variations in carbonatites. In: Bell, K. (ed.) *Carbonatites: Genesis and Evolution*. London: Unwin Hyman, pp. 301–359.

Donaldson, C. H. & Reid, A. M. (1982). Multiple intrusion of a kimberlite dyke. *Transactions of Geological Society of South Africa* **85,** 1–12.

Eggler, D. H. (1975). Peridotite–carbonate relations in the system CaO–MgO–SiO_2–CO_2. *Carnegie Institution of Washington Yearbook* **74,** 468–474.

Eggler, D. H. (1976). Composition of the partial melt of carbonated peridotite in the system CaO–MgO–SiO_2–CO_2. *Carnegie Institution of Washington Yearbook* **75,** 623–626.

Eggler, D. H. (1978). The effect of CO_2 upon partial melting of peridotite in the system Na_2O–CaO–Al_2O_3–MgO–SiO_2–CO_2 to 35 kb, with an analysis of melting in a peridotite–H_2O–CO_2 system. *American Journal of Science* **278,** 305–343.

Eggler, D. H. (1989). Carbonatites, primary melts, and mantle dynamics. In: Bell, K. (ed.) *Carbonatites: Genesis and Evolution*. London: Unwin Hyman, pp. 561–579.

Exley, R. A. & Jones, A. P. (1983). Sr^{87}/Sr^{86} in kimberlitic carbonates by ion microprobe—hydrothermal alteration, crustal contamination and relation to carbonatite. *Contributions to Mineralogy and Petrology* **83,** 288–292.

Franz, G. W. & Wyllie, P. J. (1967). Experimental studies in the system CaO–MgO–SiO_2–CO_2–H_2O. In: Wyllie, P. J. (ed.) *Ultramafic and Related Rocks*. New York: John Wiley, pp. 323–326.

Freestone, I. C. & Hamilton, D. L. (1980). The role of liquid immiscibility in the genesis of carbonatites—an experimental study. *Contributions to Mineralogy and Petrology* **73,** 105–117.

Frey, F. A., Green, D. H. & Roy, S. D. (1978). Integrated models of basalt petrogenesis: a study of quartz tholeiites to olivine melilitites from south eastern Australia utilizing geochemical and experimental petrological data. *Journal of Petrology* **19,** 463–513.

Frezzotti, M.-L., Touret, J. L. R., Lustenhouwer, W. J. & Neumann, E.-R. (1994). Melt and fluid inclusions in dunite xenoliths from La Gomera, Canary Islands: tracking the mantle metasomatic fluids. *European Journal of Mineralogy* **6,** 805–817.

Gittins, J. (1989). The origin and evolution of carbonatite magmas. In: Bell, K. (ed.) *Carbonatites: Genesis and Evolution*. London: Unwin Hyman, pp. 580–600.

Gold, D. P. (1966). The average and typical chemical composition of carbonatites. *International Mineralogical Association, Papers, Fourth General Meeting, Mineralogical Society of India*. Mysore: Mysore University Press, pp. 83–91.

Green, D. H. & Wallace, M. E. (1988). Mantle metasomatism by ephemeral carbonatite melts. *Nature* **336,** 459–462.

Haggerty, S. E. (1989). Mantle metasomes and the kinship between carbonatites and kimberlites. In: Bell, K. (ed.) *Carbonatites: Genesis and Evolution*. London: Unwin Hyman, pp. 546–560.

Hamilton, D. L. & Kjarsgaard, B. A. (1993). The immiscibility of silicate and carbonate liquids. *South African Journal of Geology* **96,** 139–142.

Harmer, R. E. & Gittins, J. (1997). The origin of dolomitic carbonatites: field and experimental constraints. *Journal of African Earth Sciences* **25,** 5–28.

Hauri, E. H., Shimizu, N., Dieu, J. J. & Hart, S. R. (1993). Evidence for hotspot-related carbonatite metasomatism in the oceanic upper mantle. *Nature* **365,** 221–227.

Huang, W.-L. & Wyllie, P. J. (1974). Eutectic between wollastonite II and calcite contrasted with thermal barrier in $MgO–SiO_2–CO_2$ at 30 kilobars, with applications to kimberlite–carbonatite petrogenesis. *Earth and Planetary Science Letters* **24,** 305–310.

Huang, W.-L. & Wyllie, P. J. (1976). Melting relationships in the systems $CaO–CO_2$ and $MgO–CO_2$ to 36 kilobars. *Geochimica et Cosmochimica Acta* **40,** 129–132.

Huang, W.-L., Wyllie, P. J. & Nehru, C. E. (1980). Subsolidus and liquidus phase relationships in the system $CaO–SiO_2–CO_2$ to 30 kbar with geological applications. *American Mineralogist* **65,** 285–301.

Ionov, D. A., Dupuy, C., O'Reilly, S. Y., Kopylova, M. G. & Genshaft, Y. S. (1993). Carbonated peridotite xenoliths from Spitsbergen: implications for trace element signature of mantle carbonate metasomatism. *Earth and Planetary Science Letters* **119,** 283–297.

Ionov, D. A., O'Reilly, S. Y., Genshaft, Y. S. & Kopylova, M. G. (1996). Carbonate-bearing mantle peridotite xenoliths from Spitsbergen: phase relationships, mineral compositions and trace-element residence. *Contributions to Mineralogy and Petrology* **125,** 375–392.

Irving, A. J. & Wyllie, P. J. (1973). Melting relationships in systems $CaO–CO_2$ and $MgO–CO_2$ to 36 kilobars, with comments on CO_2 in the mantle. *Earth and Planetary Science Letters* **20,** 220–225.

Irving, A. J. & Wyllie, P. J. (1975). Subsolidus and melting relationships for calcite, magnesite, and the join $CaCO_3–MgCO_3$ to 36 kilobars. *Geochimica et Cosmochimica Acta* **39,** 35–53.

Jones, A. P. & Wyllie, P. J. (1985). Paragenetic trends of oxide minerals in carbonate-rich kimberlites with new analyses from the Benfontein sill, South Africa. *Journal of Petrology* **26,** 210–222.

Keller, J. (1981). Carbonatite volcanism in the Kaiserstuhl alkaline complex: evidence for highly fluid carbonatitic melts at the earth's surface. *Journal of Volcanology and Geothermal Research* **9,** 423–431.

Keller, J. (1989). Extrusive carbonatites and their significance. In: Bell, K. (ed.) *Carbonatites: Genesis and Evolution*. London: Unwin Hyman, pp. 70–88.

King, B. C. & Sutherland, D. L. (1960). Alkaline rocks of eastern and southern Africa. *Science Progress* **47,** 298–321, 504–524, 709–720.

Kjarsgaard, B. A. (1997). Carbonatites in context: differentiation trends of carbonated alkaline ultrabasic silicate magmas based on field and experimental studies. *GAC–MAC Annual Meeting, Abstract Volume* A-79.

Kjarsgaard, B. A. & Hamilton, D. L. (1988). Liquid immiscibility and the origin of alkali-poor carbonatites. *Mineralogical Magazine* **52,** 43–55.

Kjarsgaard, B. A. & Hamilton, D. L. (1989*a*). The genesis of carbonatites by immiscibility. In: Bell, K. (ed.) *Carbonatites: Genesis and Evolution*. London: Unwin Hyman, pp. 388–404.

Kjarsgaard, B. A. & Hamilton, D. L. (1989*b*). Carbonatite origin and diversity. *Nature* **338,** 547–548.

Kjarsgaard, B. & Peterson, T. (1991). Nephelinite–carbonatite liquid immiscibility at Shombole Volcano, East Africa: petrographic and experimental evidence. *Mineralogy and Petrology* **43,** 293–314.

Kjarsgaard, B. A., Hamilton, D. L. & Peterson, T. D. (1995). Peralkaline nephelinite/carbonatite liquid immiscibility: comparison of phase compositions in experiments and natural lavas from Oldoinyo Lengai. In: Bell, K. & Keller, J. (eds) *Carbonatite Volcanism: Oldoinyo Lengai and the Petrogenesis of Natrocarbonatites. IAVCEI Proceedings in Volcanology 4*. Berlin: Springer-Verlag, pp. 163–190.

Kogarko, L. N., Henderson, C. M. B. & Pacheco, H. (1995). Primary Ca-rich carbonatite magma and carbonate–silicate–sulfide liquid immiscibility in the upper mantle. *Contributions to Mineralogy and Petrology* **121,** 267–274.

Koster van Groos, A. F. & Wyllie, P. J. (1966). Liquid immiscibility in the system $Na_2O–Al_2O_3–SiO_2–CO_2$ at pressures to 1 kilobar. *American Journal of Science* **264,** 234–255.

Koster van Groos, A. F. & Wyllie, P. J. (1973). Liquid immiscibility in the join $NaAlSi_3O_8–CaAl_2Si_2O_8–Na_2CO_3–H_2O$. *American Journal of Science* **273,** 465–487.

Kwon, S.-T., Tilton, G. R. & Grunenfelder, M. H. (1989). Lead isotope relationships in carbonatites and alkalic complexes: an overview. In: Bell, K. (ed.) *Carbonatites: Genesis and Evolution*. London: Unwin Hyman, pp. 360–387.

Le Bas, M. J. (1977). *Carbonatite–Nephelinite Volcanism*. London: John Wiley.

Le Bas, M. J. (1989). Diversification of carbonatite. In: Bell, K. (ed.) *Carbonatites: Genesis and Evolution*. London: Unwin Hymin, pp. 428–447.

Lee, W.-J. & Wyllie, P. J. (1992*a*). Liquid immiscibility between silicates and carbonates must intersect suitable liquidus field boundaries to have petrogenetic significance. *Abstracts, 29th International Geological Congress, Kyoto*, p. 571.

Lee, W.-J. & Wyllie, P. J. (1992*b*). Silicate–carbonate liquid miscibility gaps, and liquidus field boundaries: carbonatites by immiscibility or fractionation. *EOS Transactions, American Geophysical Union* **73,** 606.

Lee, W.-J. & Wyllie, P. J. (1994). Experimental data bearing on liquid immiscibility, crystal fractionation, and the origin of calciocarbonatites and natrocarbonatites. *International Geology Review* **36,** 797–819.

Lee, W.-J. & Wyllie, P. J. (1996). Liquid immiscibility in the join $NaAlSi_3O_8–CaCO_3$ to 2·5 GPa and the origin of calciocarbonatite magmas. *Journal of Petrology* **37,** 1125–1152.

Lee, W.-J. & Wyllie, P. J. (1997*a*). Liquid immiscibility between nephelinite and carbonatite from 2·5 to 1·0 GPa compared with mantle melt compositions. *Contributions to Mineralogy and Petrology* **127,** 1–16.

Lee, W.-J. & Wyllie, P. J. (1997*b*). Liquid immiscibility in the join $NaAlSiO_4–NaAlSi_3O_8–CaCO_3$ at 1·0 GPa: implications for crustal carbonatites. *Journal of Petrology* **38,** 1113–1135.

Lee, W.-J., Wyllie, P. J. & Rossman, G. R. (1994). CO_2-rich glass, round calcite crystals and no liquid immiscibility in the system $CaO–SiO_2–CO_2$ at 2·5 GPa. *American Mineralogist* **79,** 1135–1144.

Maaloe, S. & Wyllie, P. J. (1975). The join grossularite–calcite through the system $CaO–Al_2O_3–SiO_2–CO_2$ at 30 kilobars: crystallization range of silicates and carbonates on the liquidus. *Earth and Planetary Science Letters* **28,** 205–208.

Macdonald, R., Kjarsgaard, B. A., Skilling, I. P., Davies, G. R., Hamilton, D. L. & Black, S. (1993). Liquid immiscibility between trachyte and carbonate in ash flow tuffs from Kenya. *Contributions to Mineralogy and Petrology* **114,** 276–287.

McInnes, B. I. A. & Wyllie, P. J. (1992). Scapolite formation and the production of nephelinitic melts during the subduction of carbonated basalt. *EOS Transactions, American Geophysical Union* **73,** 637.

Mitchell, R. H. (1989). Aspects of the petrology of kimberlites and lamproites: some definitions and distinctions. In: Ross, J. (ed.) *Kimberlites and Related Rocks, Volume 1, Their Composition, Occurrence, Origin and Emplacement. Geological Society of Australia Special Publication* **14,** 7–45.

Nichols, G. T., Wyllie, P. J. & Stern, C. R. (1994). Subduction zone melting of pelagic sediments constrained by melting experiments. *Nature* **371,** 785–788.

Otto, J. W. & Wyllie, P. J. (1993). Relationships between silicate melts and carbonate-precipitating melts in $CaO–MgO–SiO_2–CO_2–H_2O$ at 2 kbar. *Mineralogy and Petrology* **48,** 343–365.

Peterson, T. D. & Kjarsgaard, B. A. (1995). What are the parental magmas at Oldoinyo Lengai? In: Bell, K. & Keller, J. (eds) *Carbonatite Volcanism: Oldoinyo Lengai and the Petrogenesis of Natrocarbonatites. IAVCEI Proceedings in Volcanology 4*. Berlin: Springer-Verlag, pp. 148–162.

Pyle, J. M. & Haggerty, S. E. (1994). Silicate–carbonate liquid immiscibility in upper-mantle eclogites: implications for natrosilicic and

carbonatitic conjugate melts. *Geochimica et Cosmochimica Acta* **58,** 2997–3011.

Rudnick, R. L., McDonough, W. F. & Chappell, B. W. (1993). Carbonatite metasomatism in the northern Tanzanian mantle—petrographic and geochemical characteristics. *Earth and Planetary Science Letters* **114,** 463–475.

Seifert, W. & Thomas, R. (1995). Silicate–carbonate immiscibility: a melt inclusion study of melilitite and wehrlite xenoliths in tephrite from the Elbe zone, Germany. *Chemie der Erde* **55,** 263–279.

Stoppa, F. & Cundari, A. (1995). A new Italian carbonatite occurrence at Cupaello (Rieti) and its genetic significance. *Contributions to Mineralogy and Petrology* **122,** 275–288.

Stoppa, F. & Lavecchia, G. (1992). Late Pleistocene ultra-alkaline magmatic activity in the Umbria–Latium region (Italy)—an overview. *Journal of Volcanology and Geothermal Research* **52,** 277–293.

Stoppa, F. & Lupini, L. (1993). Mineralogy and petrology of the Polino monticellite calciocarbonatite (central Italy). *Mineralogy and Petrology* **49,** 213–231.

Sweeney, R. J. (1994). Carbonatite melt compositions in the Earth's mantle. *Earth and Planetary Science Letters* **128,** 259–270.

Sweeney, R. J., Green, D. H. & Sie, S. H. (1992). Trace and minor element partitioning between garnet and amphibole and carbonatitic melt. *Earth and Planetary Science Letters* **113,** 1–14.

Thibault, Y., Edgar, A. D. & Lloyd, F. E. (1992). Experimental investigation of melts from a carbonated phlogopite lherzolite: implications for metasomatism in the continental lithospheric mantle. *American Mineralogist* **77,** 784–794.

Treiman, A. H. & Essene, E. J. (1985). The Oka carbonatite complex, Quebec: geology and evidence for silicate–carbonate liquid immiscibility. *American Mineralogist* **70,** 1101–1113.

Wallace, M. E. & Green, D. H. (1988). An experimental determination of primary carbonatite magma composition. *Nature* **335,** 343–346.

Watkinson, D. H. & Wyllie, P. J. (1971). Experimental study of the join $NaAlSiO_4$–$CaCO_3$–H_2O and the genesis of alkalic rock–carbonatite complexes. *Journal of Petrology* **12,** 357–378.

Wendlandt, R. F. & Eggler, D. H. (1980*a*). The origins of potassic magmas. 1. Melting relations in the systems $KAlSiO_4$–Mg_2SiO_4–SiO_2 and $KAlSiO_4$–MgO–SiO_2–CO_2 to 30 kilobars. *American Journal of Science* **280,** 385–420.

Wendlandt, R. F. & Eggler, D. H. (1980*b*). The origins of potassic magmas. 2. Stability of phlogopite in natural spinel lherzolite and in the system $KAlSiO_4$–MgO–SiO_2–H_2O–CO_2 at high pressures and high temperatures. *American Journal of Science* **280,** 421–458.

Woolley, A. R. & Kempe, D. R. C. (1989). Carbonatites: nomenclature, average chemical compositions, and element distribution. In: Bell, K. (ed.) *Carbonatites: Genesis and Evolution*. London: Unwin Hyman, pp. 1–14.

Wyllie, P. J. (1977). Mantle fluid compositions buffered by carbonates in peridotite–CO_2–H_2O. *Journal of Geology* **85,** 187–207.

Wyllie, P. J. (1978). Mantle fluid compositions buffered in peridotite–CO_2–H_2O by carbonates, amphibole, and phlogopite. *Journal of Geology* **86,** 687–713.

Wyllie, P. J. (1987). Transfer of subcratonic carbon into kimberlites and rare earth carbonatites. In: Mysen, B. O. (ed.) *Magmatic Processes: Physicochemical Principles. Geochemical Society, Special Publication* **1,** 107–119.

Wyllie, P. J. & Huang, W.-L. (1975). Peridotite, kimberlite, and carbonatite explained in the system CaO–MgO–SiO_2–CO_2. *Geology* **3,** 621–624.

Wyllie, P. J. & Huang, W.-L. (1976*a*). Carbonation and melting reactions in the system CaO–MgO–SiO_2–CO_2 at mantle pressures with geophysical and petrological applications. *Contributions to Mineralogy and Petrology* **54,** 79–107.

Wyllie, P. J. & Huang, W.-L. (1976*b*). High CO_2 solubilities in mantle magmas. *Geology* **4,** 21–24.

Wyllie, P. J. & Rutter, M. (1986). Experimental data on the solidus of peridotite–CO_2, with applications to alkaline magmatism and mantle metasomatism. *EOS Transactions, American Geophysical Union* **67,** 390.

Wyllie, P. J. & Tuttle, O. F. (1960). The system CaO–CO_2–H_2O and the origin of carbonatites. *Journal of Petrology* **1,** 1–46.

Wyllie, P. J., Huang, W.-L., Otto, J. & Byrnes, A. P. (1983). Carbonation of peridotites and decarbonation of siliceous dolomites represented in the system CaO–MgO–SiO_2–CO_2 to 30 kbar. *Tectonophysics* **100,** 359–388.

Yaxley, G. M. & Green, D. H. (1996). Experimental reconstruction of sodic dolomitic carbonatite melts from metasomatised lithosphere. *Contributions to Mineralogy and Petrology* **124,** 359–369.

Yaxley, G. M., Crawford, A. J. & Green, D. H. (1991). Evidence for carbonatite metasomatism in spinel peridotite xenoliths from western Victoria, Australia. *Earth and Planetary Science Letters* **107,** 305–317.